AD-A055 381 AIR FORCE FLIGHT DYNAMICS LAB WRIGHT-PATTERSON AFB OHIO F/G 1/2
OPTIMAL FLARE WITH WIND DISTURBANCES.(U)
APR 77 B G KUNCIW

UNCLASSIFIED AFFDL-TR-77-15 NL

| OF |
ADA
055381

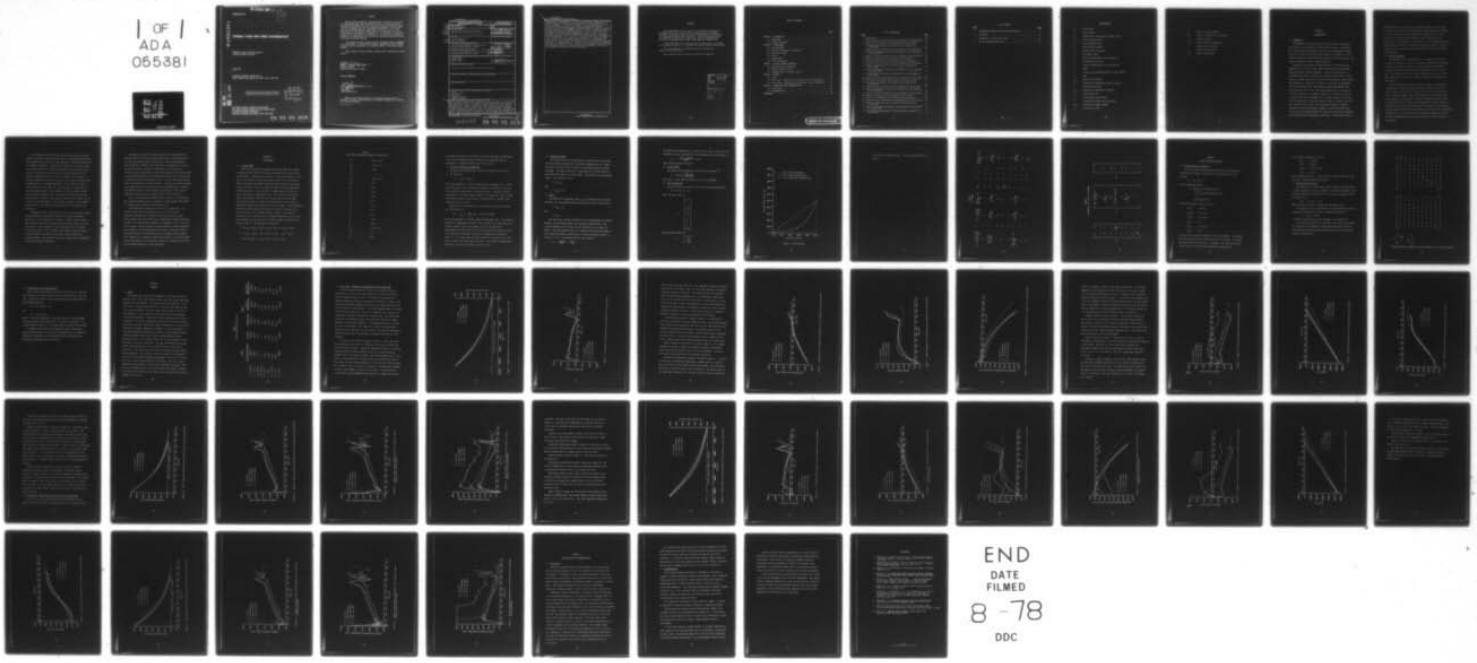

END
DATE
FILMED
8-78
DDC

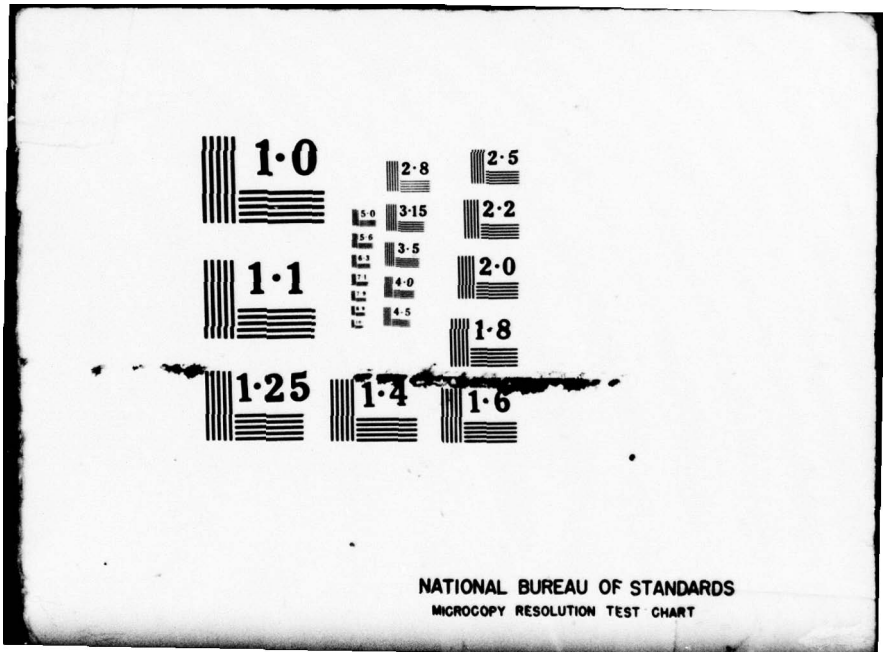
1·0
1·1
1·25
1·4
1·6
2·8
3·15
3·5
4·0
4·5
5·0
2·5
2·2
2·0
1·8
NATIONAL BUREAU OF STANDARDS
MICROCOPY RESOLUTION TEST CHART

AFFDL-TR-77-15

OPTIMAL FLARE WITH WIND DISTURBANCES

TERMINAL AREA CONTROL BRANCH
FLIGHT CONTROL DIVISION

APRIL 1977

TECHNICAL REPORT AFFDL-TR-77-15
FINAL REPORT FOR PERIOD JANUARY 1975 to JUNE 1976

AIR FORCE FLIGHT DYNAMICS LABORATORY
AIR FORCE WRIGHT AERONAUTICAL LABORATORIES
AIR FORCE SYSTEMS COMMAND
WRIGHT-PATTERSON AIR FORCE BASE, OHIO 45433

NOTICE

When Government drawings, specifications, or other data are used for any purpose other than in connection with a definitely related Government procurement operation, the United States Government thereby incurs no responsibility nor any obligation whatsoever; and the fact that the Government may have formulated, furnished, or in any way supplied the said drawings, specifications, or other data, is not to be regarded by implication or otherwise as in any manner licensing the holder or any other person or corporation, or conveying any rights or permission to manufacture, use, or sell any patented invention that may in any way be related thereto.

This report has been reviewed by the Information Office (ASD/OIP) and is releasable to the National Technical Information Service (NTIS). At NTIS it will be available to the general public, including foreign nations.

This technical report has been reviewed and is approved for publication.

Bohdan G. Kunciw

BOHDAN G. KUNCIW, Capt, USAF
Project Engineer
Terminal Area Control Branch

FOR THE COMMANDER

R P Johannes

R. P. JOHANNES
Acting Chief
Flight Control Division

Copies of this report should not be returned unless return is required by security considerations, contractual obligations, or notice on a specific document.

AIR FORCE - 28 JUN 77 - 300

UNCLASSIFIED

SECURITY CLASSIFICATION OF THIS PAGE (When Data Entered)

REPORT DOCUMENTATION PAGE

READ INSTRUCTIONS BEFORE COMPLETING FORM

1. REPORT NUMBER: AFFDL-TR-77-15	2. GOVT ACCESSION NO.
3. RECIPIENT'S CATALOG NUMBER	
4. TITLE (and Subtitle): Optimal Flare with Wind Disturbances.	5. TYPE OF REPORT & PERIOD COVERED: Final Report for Period Jan 1975 - Jun 1976
6. PERFORMING ORG. REPORT NUMBER	
7. AUTHOR(s): Bohdan G. Kunciw	8. CONTRACT OR GRANT NUMBER(s)
9. PERFORMING ORGANIZATION NAME AND ADDRESS: Air Force Flight Dynamics Laboratory (FGT), Wright-Patterson AFB, Ohio 45433	10. PROGRAM ELEMENT, PROJECT, TASK AREA & WORK UNIT NUMBERS: 62201F, 82260140
11. CONTROLLING OFFICE NAME AND ADDRESS: Air Force Flight Dynamics Laboratory (FGT), Wright-Patterson AFB, Ohio 45433	12. REPORT DATE: April 1977
	13. NUMBER OF PAGES: 53
14. MONITORING AGENCY NAME & ADDRESS (if different from Controlling Office): 63p.	15. SECURITY CLASS. (of this report): UNCLASSIFIED
	15a. DECLASSIFICATION/DOWNGRADING SCHEDULE: N/A

16. DISTRIBUTION STATEMENT (of this Report)

Approved for public release; distribution unlimited.

17. DISTRIBUTION STATEMENT (of the abstract entered in Block 20, if different from Report)

18. SUPPLEMENTARY NOTES

19. KEY WORDS (Continue on reverse side if necessary and identify by block number)

Flare
Optimal Control
Wind Shear
Terminal Controller
Automatic Landing

20. ABSTRACT (Continue on reverse side if necessary and identify by block number)

A linear optimal control law is developed to flare an aircraft, in constant wind and wind shear conditions, with minimal touchdown longitudinal range and sink rate dispersions. Range is included as a state variable in order to specify a touchdown point. Control variables are control column and throttle movement. In-flight constraints are placed on pitch rate, normal airspeed, longitudinal airspeed, and elevator angle; this permits a smooth profile with a gradual speed bleed. Terminal constraints are placed on pitch rate, longitudinal airspeed, thrust, range, sink rate, and altitude; this yields minimal range and sink rate → next page B

DD FORM 1 JAN 73 1473 EDITION OF 1 NOV 65 IS OBSOLETE

UNCLASSIFIED

SECURITY CLASSIFICATION OF THIS PAGE (When Data Entered)

dispersions with acceptable aircraft states at touchdown. Optimal time varying feedback gains are obtained for a no-wind condition; they are good for any initial conditions. Since flare time changes in wind conditions, the no wind gains are scheduled as a function of range. Wind and ground effect are considered to be disturbances. The following headwinds are simulated: constant 30 knots from 1000 to 10 feet above the ground, constant 30 knots from 1000 to 510 feet and then linearly shears to 0 knots at 10 feet, and constant 30 knots from 1000 to 510 feet and then logarithmically shears to 0 knots at 10 feet. The optimal control law yielded smooth flare trajectories with a longitudinal touchdown dispersion of only 71.1 feet and sink rate dispersion at touchdown of only .17 feet/second. As a comparison, a simulation of a conventional operational autopilot in the same wind conditions resulted in a longitudinal dispersion of 2017 feet and sink rate dispersion of 5.55 feet/second with a maximum sink rate of -6.2 feet/second. The optimal control technique can be extended to placing an air vehicle at any point in space, with any terminal conditions, with any in-flight constraints, in any deterministic wind conditions; this can be done regardless of the vehicle's initial conditions.

FOREWORD

This report describes the results of an in-house investigation to develop an aircraft flare control law which would have minimal touchdown longitudinal range and sink rate dispersions in the presence of constant and shearing wind conditions. Time varying optimal gains are scheduled on the basis of range from a desired touchdown point. The work was performed under Project 8226, Task 01, Work Unit 40.

Sincere appreciation for their technical consultations is extended to Dr. Robert R. Huber, Jr., Capt Robert P. Denaro, and Mr. Thomas Imrich.

This investigation was performed during the period from January 1975 to June 1976.

This technical report has been reviewed and is approved.

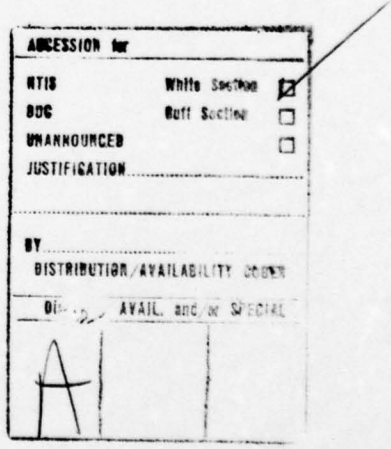

TABLE OF CONTENTS

	Page
SECTION 1 INTRODUCTION	1
1.1 Background	1
1.2 Analysis Technique	2
SECTION 2 SYSTEM MODEL	5
2.1 Aircraft Model	5
2.2 Elevator and Engine Lag Equations	7
2.3 Position in Space	8
2.4 Winds	8
2.5 Ground Effect	9
2.6 Full System Model	9
SECTION 3 OPTIMAL CONTROL TECHNIQUE	14
3.1 Optimal Control Formulation	14
3.2 Optimal Control Solution	15
3.3 Implementation of Optimal Solution	17
SECTION 4 RESULTS	18
4.1 Scope	18
4.2 First Case: Simulation with Identical Initial Conditions	20
4.3 Second Case: Simulation with Different Initial Conditions	31
SECTION 5 CONCLUSIONS AND RECOMMENDATIONS	50
5.1 Conclusions	50
5.2 Recommendations	51
REFERENCES	53

LIST OF ILLUSTRATIONS

Figure		Page
1	Wind Profiles	10
2	Range Trajectories with Identical Initial Conditions for Various Winds	21
3	Pitch Rates with Identical Initial Conditions for Various Winds	22
4	Perturbation Pitch Angles with Identical Initial Conditions for Various Winds	24
5	Normal Airspeeds with Identical Initial Conditions for Various Winds	25
6	Perturbation Longitudinal Airspeeds with Identical Initial Conditions for Various Winds	26
7	Changes in Thrust with Identical Initial Conditions for Various Winds	28
8	Ranges with Identical Initial Conditions for Various Winds	29
9	Sink Rates with Identical Initial Conditions for Various Winds	30
10	Time Trajectories with Identical Initial Conditions for Various Winds	32
11	Changes in Elevator Angle with Identical Initial Conditions for Various Winds	33
12	Control Column Angular Displacements with Identical Initial Conditions for Various Winds	34
13	Throttle Angular Displacements with Identical Initial Conditions for Various Winds	35
14	Range Trajectories with Different Initial Conditions for Various Winds	37
15	Pitch Rates with Different Initial Conditions for Various Winds	38
16	Perturbation Pitch Angles with Different Initial Conditions for Various Winds	39
17	Normal Airspeeds with Different Initial Conditions for Various Winds	40
18	Perturbation Longitudinal Airspeeds with Different Initial Conditions for Various Winds	41
19	Changes in Thrust with Different Initial Conditions for Various Winds	42
20	Ranges with Different Initial Conditions for Various Winds	43
21	Sink Rates with Different Initial Conditions for Various Winds	45
22	Time Trajectories with Different Initial Conditions for Various Winds	46
23	Changes in Elevator Angle with Different Initial Conditions for Various Winds	47
24	Control Column Angular Displacements with Different Initial Conditions for Various Winds	48
25	Throttle Angular Displacements with Different Initial Conditions for Various Winds	49

LIST OF TABLES

Table		Page
1	Longitudinal Dimensional Stability Derivatives	6
2	"A" Matrix	12
3	"B" Matrix, "d_1" and "d_2" Vectors	13
4	Initial Conditions for Flare	19

NOMENCLATURE

A	system matrix
B	control matrix
d_1	ground effect and system's constants vector
d_2	wind disturbance vector
F	system feedback matrix
H	ground effect parameter
h	altitude above the ground
J	performance index
Q	state weighting matrix in cost function
q	perturbation pitch rate
R	control weighting matrix in cost function
r	range
S	terminal state weighting matrix in cost function
t	time
U_o	steady state airspeed
u	perturbation longitudinal inertial velocity
$\underline{u}$	system control vector
u_{as}	perturbation longitudinal airspeed
u_w	longitudinal wind
$\underline{v}$	system optimal input vector
w	perturbation normal inertial velocity
w_{as}	perturbation normal airspeed
$\underline{x}$	system state vector

δe	change in elevator angle
δe_c	control column angular displacement
δT	change in thrust
δth_c	throttle angular displacement
θ	perturbation pitch angle
τ_e	elevator time constant
τ_{th}	engine time constant

SECTION 1

INTRODUCTION

1.1 Background

Investigations of several recent aircraft accidents indicate that wind shear is a factor which can cause aircraft crashes. One accident was a crash during an ILS approach of Iberia Airlines McDonnell Douglas DC 10-30 at Logan International Airport, Boston, on December 17, 1973.[1] Another accident was an Eastern Airlines Boeing 727 crash on June 24, 1975 during an approach to John F. Kennedy Airport.[2]

During this time frame, the "Speckled Trout" C-135A flight test program at the Air Force Flight Dynamics Laboratory was investigating advanced automatic landing techniques. Various inconsistencies in performance were noted. Wind shear was suspected as the cause. Consequently, a hybrid simulation of the aircraft and automatic control system was undertaken to investigate the effects of wind shear on performance. This study indicated that a logarithmically decreasing headwind from 50.67 ft/sec (30 kt) at 510 ft AGL (above ground level) to 0 ft/sec at 10 ft AGL resulted in an automatic landing 721 ft short of the no wind case and a sink rate at touchdown of -6.2 ft/sec instead of -2.1 ft/sec for the no wind case.[3] From an altitude of 1000 ft to 510 ft, the wind was a constant 50.67 ft/sec. This particular wind shear condition resulted in the worst performance compared to steady state winds and linear shears of comparable magnitude (logarithmic winds were considered more representative of atmospheric conditions). Considering the above

logarithmic shear, a similar 30 kt headwind shear which is linear, and a constant 30 kt headwind, the longitudinal range dispersion at touchdown was 2017 ft and the sink rate dispersion at touchdown was 5.55 ft/sec. Dispersion is the span from the minimum to the maximum values; each extreme limit is determined by a wind condition. The longitudinal control equations were based on the conventional operational autopilot installed in the aircraft; during the time based exponential flare, the throttles retard linearly.

1.2 Analysis Technique

The objective of this investigation is to design a flare control law that will enable an aircraft on an automatic approach in the presence of unknown wind shears to achieve the smallest possible longitudinal dispersion and sink rate deviation at touchdown relative to a no wind case. The flare portion of the automatic landing was chosen since the flare control law is a major cause of poor landings in the presence of wind shears.[3]

The best possible performance should be obtained by using optimal control theory. Nonlinear equations of motion cannot be used since a control law has to be obtained for every new set of initial conditions and the computation speed is not great enough for real time application. Linear equations of motion with a quadratic performance integral permit a solution which yields a control law independent of initial conditions; the optimal control gains are fixed prior to installation of an automatic landing system in an aircraft and are valid for any flare initial conditions. In application, of course, these initial conditions should fall within a broad set of appropriate flare initial conditions to ensure acceptable trajectories.

Linear optimal control solutions for flare have been investigated. However, the effects of arbitrary wind shears on longitudinal dispersions and touchdown sink rates have not been addressed. Merriam[4] and Neal[5] did not consider wind effects. Applying their optimal control gains, which are functions of time, in a wind environment will not yield satisfactory results. Dispersions and sink rates will change considerably in the presence of winds since the air mass is in motion. As an example, a constant headwind will cause the aircraft to be further from the no wind touchdown point at a corresponding point in time. Huber[6] included a linear wind shear in his work; but, the wind shear was known a priori. The wind shear was placed in the equations of motion; optimal control gains reflected a specific wind. The solution is valid for only that wind condition. Trankle[7] used an optimal regulator with integral control to track an altitude profile. This technique, however, can only handle constant winds. The results are not satisfactory if wind shears are introduced.

The approach in this investigation was to use linear optimal control theory and model the performance index after a pilot's performance. Specifically, a trajectory was not tracked. Instead, terminal weights were placed on pitch rate, airspeed, thrust, touchdown point, sink rate, and altitude. Since airspeed is critical during flare, an airspeed profile was tracked. Also, in order to keep normal acceleration small, in-flight weights were placed on pitch rate, normal airspeed, and elevator position. The controls were control column angular displacement and throttle angular displacement.

Furthermore, a crucial difference between this investigation and previous work that used time varying optimal gains is the application of the time varying gains based on range from a no wind touchdown point. This scheduling is feasible since range from a touchdown point is one of the aircraft states. Range may be determined in the future from a microwave landing system (MLS) or global positioning satellite system (GPS). As was mentioned previously, gain scheduling based on time in the presence of wind does not yield satisfactory results. In this study, time varying gains are obtained for a no wind condition. The gains are stored according to the range of the aircraft from the no wind touchdown point. Constant wind and wind shears are then treated as disturbances to the system in simulations of the aircraft using the optimal no wind control law.

Also, in the simulations, ground effect is treated as a disturbance. But, unlike wind which cannot be predicted, a nominal ground effect model is included in the solution for the optimal gains.

A CDC 6600 digital computer was used for all computations. The optimal control gains and simulation are for a C-135A aircraft. Simulation indicated that the optimal control gains based on range provide smooth flare trajectories with a longitudinal touchdown dispersion of only 71.1 ft and sink rate dispersion at touchdown of only .17 ft/sec. 30 kt constant, linearly shearing, and logarithmically shearing headwinds were included in this investigation; these winds are the same as those mentioned previously in the discussion of the "Speckled Trout" program. Thus, compared to a conventional operational autopilot, the linear optimal control law permits a very significant reduction in longitudinal and sink rate touchdown dispersions in wind conditions.

SECTION 2

SYSTEM MODEL

2.1 Aircraft Model

Linearized longitudinal equations for perturbations about trimmed straight and level flight in a landing configuration were used for the aircraft model. Stability axes were used: right hand coordinate system with x axis along the steady state velocity vector and z axis pointed down.[8] The steady state values for pitch angle, pitch rate, and normal inertial velocity are zero. It should be noted that even though steady state pitch angle is zero, the nose is slightly high in straight and level flight for the configuration used. The aircraft's pitch angle is equal to perturbation pitch plus the straight and level pitch angle. The actual pitch angle is needed to indicate whether or not the main landing gear impacts the ground prior to the nose wheel. The perturbation pitch rate and perturbation normal inertial velocity are equal to the aircraft's pitch rate and normal inertial velocity. The stability derivatives for a C-135A aircraft in landing configuration with a steady state airspeed, U_o, of 261.8 ft/sec and gross weight of 160,000 lbs are listed in Table 1. The equations of motion are[9]

$$\ddot{\theta} = M_w w_{as} + M_{\dot{w}} \dot{w}_{as} + M_q \dot{\theta} + M_u u_{as} + M_{\delta T} \delta T + M_{\delta e} \delta e + M_H H$$

$$\dot{w} = Z_w w_{as} + Z_{\dot{w}} \dot{w}_{as} + (U_o + Z_q) \dot{\theta} + Z_u u_{as} + Z_{\delta e} \delta e + Z_H H$$

$$\dot{u} = -g\theta + X_w w_{as} + X_u u_{as} + X_{\delta T} \delta T + X_{\delta e} \delta e + X_H H.$$

TABLE 1

LONGITUDINAL DIMENSIONAL STABILITY DERIVATIVES[9]

M_w	$-.6916 \times 10^{-2}$
$M_{\dot{w}}$	$-.1466 \times 10^{-2}$
M_q	-.9512
M_u	0
$M_{\delta T}$	$.1852 \times 10^{-5}$
$M_{\delta e}$	1.390
M_H	-.2576
Z_w	-.708
$Z_{\dot{w}}$	-.0105
Z_q	-6.84
Z_u	-.302
$Z_{\delta e}$	9.23
Z_H	-5.113
X_w	.0719
X_u	-.0474
$X_{\delta T}$	$.2013 \times 10^{-3}$
$X_{\delta e}$	1.84
X_H	1.812

It should be noted that the variables on the left hand side are referenced to an inertial reference frame and those on the right hand side are referenced to a reference frame fixed in the air mass.

2.2 Elevator and Engine Lag Equations

Elevator lag was modelled as a first order lag with time constant τ_e. The equation is

$$\dot{\delta e} = -\frac{1}{\tau_e}\,\delta e + \frac{1}{\tau_e}\,\delta e_c.$$

The control parameter is control column angular displacement, δe_c. Change in elevator angle is δe; up elevator is positive. Deflection is relative to the stabilizer which moves to trim the aircraft. Stabilizer trim was not modelled; its position remains fixed at its steady state value. Steady state elevator angle is zero relative to the stabilizer. Elevator time constant was set at 1/3 sec.

Engine lag was also modelled as a first order lag with time constant τ_{th}. The equation is

$$\dot{\delta T} = -\frac{1}{\tau_{th}}\,\delta T + \frac{750}{\tau_{th}}\,\delta th_c - (31.39)(1.5)(750).$$

The control parameter is throttle angular displacement, δth_c. Full throttle deflection is approximately 48 deg. The last term on the right hand side is needed in order to specify idle thrust level for the throttle at approximately zero deg. The 750 in the second term on the right hand side of the equation is necessary to get units of pounds for the change in thrust, δT. δT is the change in thrust relative to the steady state value which is half of the total thrust available. Total thrust is approximately 48,000 lbs. The time constant was set at 1/1.5 sec.

2.3 Position in Space

The inertial location of the aircraft is specified by its altitude above the ground and range from a specified touchdown point on a runway. The center of gravity of the aircraft is the reference point for these variables. The center of gravity is considered to be 10 feet above the ground when the aircraft is on the runway. The equations for determining range, r, and altitude, h, are

$$\dot{r} = U_o + u$$

and

$$\ddot{h} = U_o \dot{\theta} - \dot{w}.$$

2.4 Winds

The effects of longitudinal winds, u_w, are considered in this study. Therefore, the relationships between inertial and air mass velocities are

$$u = u_{as} + u_w$$

and

$$w = w_{as}.$$

The three types of winds considered in this investigation are constant headwind, linear headwind shear, and logarithmic headwind shear. The constant headwind is 50.67 ft/sec (30 kt) from 1000 to 10 ft above the ground. The linear headwind shear is a constant 50.67 ft/sec from 1000 to 510 ft above the ground, at which point it starts decreasing linearly to 0 ft/sec at 10 ft. The equation for the linear shear is

$$u_w = -\frac{50.67\ h}{500} + \frac{50.67}{50}.$$

The logarithmic headwind shear is similar to the linear, except that the headwind decreases logarithmically. The equation for this wind shear is

$$u_w = - \frac{50.67 \ln(h/510)}{\ln(51)} - 50.67.$$

These winds are shown in Figure 1.

2.5 Ground Effect

The ground effect parameter, H, for the C-135 aircraft is[9]

$$H = .0139 \exp \left[\frac{120 - h}{30.6818} \right] .$$

This model is valid from an altitude of 120 ft to touchdown.

2.6 Full System Model

Using the previous equations, the full system may be described by

$$\dot{\underline{x}} = A\underline{x} + B\underline{u} + \underline{d}_1 + \underline{d}_2$$

where the state vector is

$$\underline{x} = \begin{bmatrix} q \\ \theta \\ w_{as} \\ u_{as} \\ \delta T \\ r \\ \dot{h} \\ h \\ \delta e \end{bmatrix}$$

and the control vector is

$$\underline{u} = \begin{bmatrix} \delta e_c \\ \delta th_c \end{bmatrix}$$

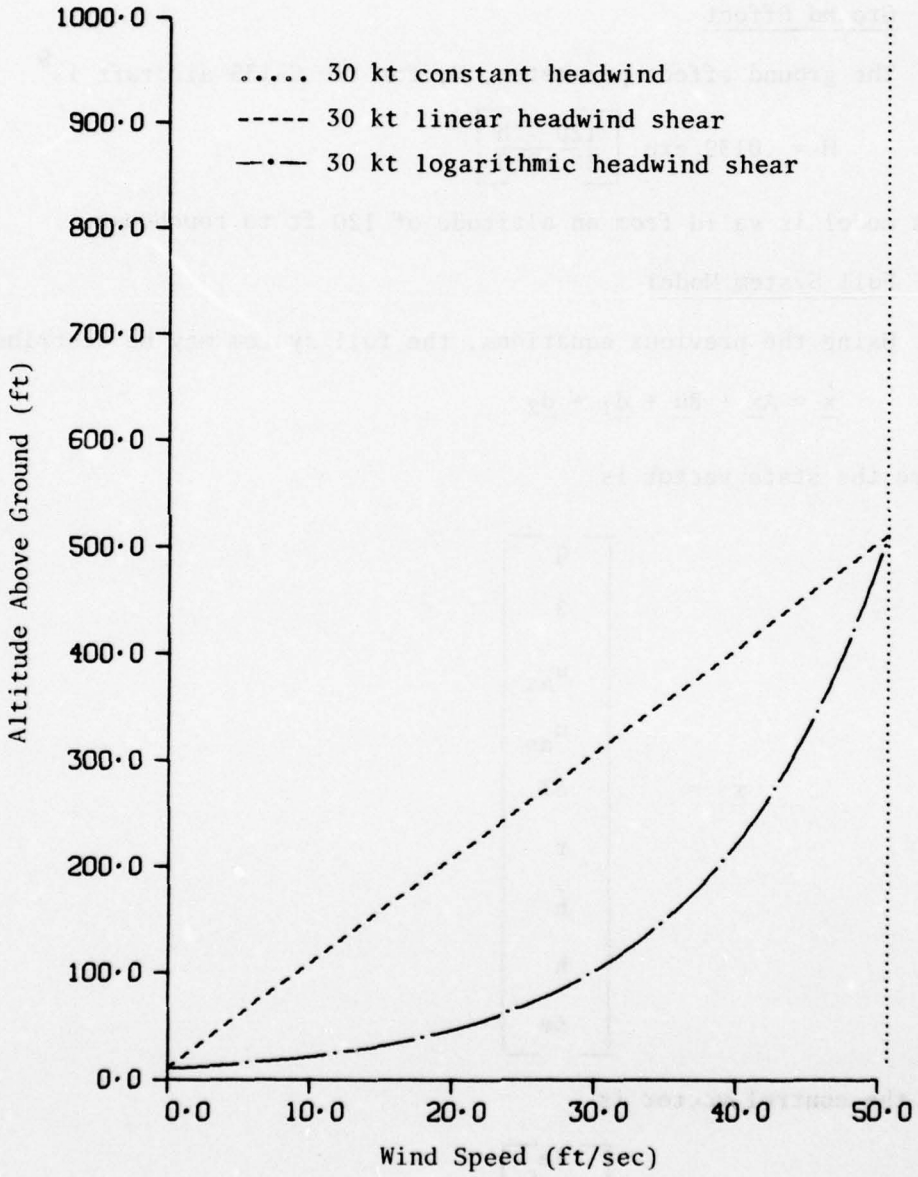

Figure 1. Wind Profiles

The A matrix is given in Table 2. B, $\underline{d}_1$, and $\underline{d}_2$ are given in Table 3.

TABLE 2

"A" MATRIX

$$
\begin{bmatrix}
M_q + M_{\dot{w}} \dfrac{(U_o + Z_q)}{(1 - Z_{\dot{w}})} & 0 & M_w + \dfrac{M_{\dot{w}} Z_w}{(1 - Z_{\dot{w}})} & \dfrac{M_{\dot{w}} Z_u}{(1 - Z_{\dot{w}})} + M_u & M_{\delta T} & 0 & 0 & 0 & \dfrac{M_{\dot{w}} Z_{\delta e}}{(1 - Z_{\dot{w}})} + M_{\delta e} \\
1 & 0 & 0 & 0 & 0 & 0 & 0 & 0 & 0 \\
\dfrac{(U_o + Z_q)}{(1 - Z_{\dot{w}})} & 0 & \dfrac{Z_w}{(1 - Z_{\dot{w}})} & \dfrac{Z_u}{(1 - Z_{\dot{w}})} & 0 & 0 & 0 & 0 & \dfrac{Z_{\delta e}}{(1 - Z_{\dot{w}})} \\
0 & -g & X_w & X_u & X_{\delta T} & 0 & 0 & 0 & X_{\delta e} \\
0 & 0 & 0 & 0 & -\dfrac{1}{\tau_{th}} & 0 & 0 & 0 & 0 \\
0 & 0 & 0 & 1 & 0 & 0 & 0 & 0 & 0 \\
-\dfrac{(U_o + Z_q)}{(1 - Z_{\dot{w}})} + U_o & 0 & -\dfrac{Z_w}{(1 - Z_{\dot{w}})} & -\dfrac{Z_u}{(1 - Z_{\dot{w}})} & 0 & 0 & 0 & 0 & -\dfrac{Z_{\delta e}}{(1 - Z_{\dot{w}})} \\
0 & 0 & 0 & 0 & 0 & 0 & 1 & 0 & 0 \\
0 & 0 & 0 & 0 & 0 & 0 & 0 & 0 & -\dfrac{1}{\tau_e}
\end{bmatrix}
$$

TABLE 3

"B" MATRIX, "d_1" and "d_2" VECTORS

$$B = \begin{bmatrix} 0 & 0 \\ 0 & 0 \\ 0 & 0 \\ 0 & 0 \\ 0 & \frac{750}{\tau_{th}} \\ 0 & 0 \\ 0 & 0 \\ 0 & 0 \\ \frac{1}{\tau_e} & 0 \end{bmatrix} \qquad d_1 = \begin{bmatrix} (M_H + \frac{M_{\dot{w}} Z_H}{1 - Z_{\dot{w}}}) (H) \\ 0 \\ \frac{Z_H}{1 - Z_{\dot{w}}} H \\ X_H H \\ -(31.39)(1.5)(750) \\ U_o \\ -\frac{Z_H}{1 - Z_{\dot{w}}} H \\ 0 \\ 0 \end{bmatrix} \qquad d_2 = \begin{bmatrix} 0 \\ 0 \\ 0 \\ -\dot{u}_w \\ 0 \\ u_w \\ 0 \\ 0 \\ 0 \end{bmatrix}$$

SECTION 3

OPTIMAL CONTROL TECHNIQUE

3.1 Optimal Control Formulation

The linear optimal control problem for the no wind system with terminal and in-flight constraints may be described by the state equation

$$\dot{\underline{x}} = A\underline{x} + B\underline{u} + \underline{d}_1$$

and the performance index

$$J = \tfrac{1}{2}[\underline{x}(t_f)-\underline{r}(t_f)]^T S[\underline{x}(t_f)-\underline{r}(t_f)] + \tfrac{1}{2}\int_{t_o}^{t_f}\{[\underline{x}(t)-\underline{r}(t)]^T Q(t)[\underline{x}(t)-\underline{r}(t)] + \underline{u}^T(t)R(t)\underline{u}(t)\}dt.$$

The desired terminal values, $\underline{r}(t_f)$, are

$$q(t_f) = 0 \text{ rad/sec}$$

$$u_{as}(t_f) = -13.8 \text{ ft/sec}$$

$$\delta T(t_f) = -23{,}540 \text{ lbs}$$

$$r(t_f) = 0 \text{ ft}$$

$$\dot{h}(t_f) = -2.5 \text{ ft/sec}$$

$$h(t_f) = 10 \text{ ft.}$$

The pitch rate constraint minimizes rotation at touchdown. The airspeed and sink rate specified are desired for the C-135 aircraft. The thrust constraint specifies idle thrust at touchdown. The range and altitude values identify a desired ground referenced touchdown point.

The in-flight constraints, r(t), are

$$q(t) = 0 \text{ rad/sec}$$

$$w(t) = 0 \text{ ft/sec}$$

$$u_{as}(t) = -.191t^2 \text{ ft/sec}$$

$$\delta e(t) = 0 \text{ rad.}$$

These constraints specify a trajectory with a smooth arresting of sink rate and a designated speed bleed profile.

3.2 Optimal Control Solution

The solution to a linear optimal control problem with terminal and in-flight constraints is given by Huber.[6] He extends the optimal linear tracking technique discussed by Kirk[10] to include a disturbance vector. The control law is

$$\underline{u}(t) = F(t)\ \underline{x}(t) + \underline{v}(t).$$

Huber discusses in detail a technique for obtaining F and $\underline{v}$.

In determining F and $\underline{v}$, ground effect was approximated by using the following altitude profile in order to completely specify $\underline{d}_1$:

$$h = 70 \exp(-.255t).$$

It should be noted that $\underline{d}_2$ was not included in the computation.

With the optimal control law specified, the no wind state equation was integrated by implementing a fourth-order Runge-Kutta algorithm. The weights which resulted in the best adherence to the in-flight and terminal constraints are

$$S = \begin{bmatrix} 10^8 & 0 & 0 & 0 & 0 & 0 & 0 & 0 & 0 \\ 0 & 0 & 0 & 0 & 0 & 0 & 0 & 0 & 0 \\ 0 & 0 & 0 & 0 & 0 & 0 & 0 & 0 & 0 \\ 0 & 0 & 0 & 10^6 & 0 & 0 & 0 & 0 & 0 \\ 0 & 0 & 0 & 0 & 10^2 & 0 & 0 & 0 & 0 \\ 0 & 0 & 0 & 0 & 0 & 10^2 & 0 & 0 & 0 \\ 0 & 0 & 0 & 0 & 0 & 0 & 10^6 & 0 & 0 \\ 0 & 0 & 0 & 0 & 0 & 0 & 0 & 10^6 & 0 \\ 0 & 0 & 0 & 0 & 0 & 0 & 0 & 0 & 0 \end{bmatrix}$$

$$Q = \begin{bmatrix} 10^4 & 0 & 0 & 0 & 0 & 0 & 0 & 0 & 0 \\ 0 & 0 & 0 & 0 & 0 & 0 & 0 & 0 & 0 \\ 0 & 0 & 10^4 & 0 & 0 & 0 & 0 & 0 & 0 \\ 0 & 0 & 0 & 10^6 & 0 & 0 & 0 & 0 & 0 \\ 0 & 0 & 0 & 0 & 0 & 0 & 0 & 0 & 0 \\ 0 & 0 & 0 & 0 & 0 & 0 & 0 & 0 & 0 \\ 0 & 0 & 0 & 0 & 0 & 0 & 0 & 0 & 0 \\ 0 & 0 & 0 & 0 & 0 & 0 & 0 & 0 & 0 \\ 0 & 0 & 0 & 0 & 0 & 0 & 0 & 0 & 10^4 \end{bmatrix}$$

$$R = \begin{bmatrix} 5X10^6 & 0 \\ 0 & 10^3 \end{bmatrix}.$$

A CDC 6600 digital computer was used to perform all of the calculations.

3.3 Implementation of Optimal Solution

Based on the no wind optimal solution, F(t) and $\underline{v}(t)$ were tabulated with respect to the range associated with each time interval: F(r) and $\underline{v}(r)$. Simulation of flare in wind conditions was then accomplished with the following equations:

$$\dot{\underline{x}} = A\underline{x} + B\underline{u} + \underline{d}_1 + \underline{d}_2$$

and

$$\underline{u} = F(r)\ \underline{x} + \underline{v}(r)$$

where r is the state specified in the state vector $\underline{x}$. The disturbance vector $\underline{d}_1$ includes ground effect which is a function of altitude. The wind disturbance vector, $\underline{d}_2$, is also specified as a function of altitude.

It should be noted that the in-flight and terminal constraints, along with their weights, were not fully determined prior to simulation with winds. Simulation in wind conditions aided in identifying the constraints and weights that were selected.

SECTION 4

RESULTS

4.1 Scope

The optimal flare control law was applied in 50.67 ft/sec constant headwind, 50.67 ft/sec linear headwind shear, and 50.67 ft/sec logarithmic headwind shear environments. Two distinct cases were simulated. In the first case, the initial conditions for all the states were kept the same for all wind conditions; the initial values were the same as for the no wind condition. In the second case, the initial values were different for each wind condition. In both cases, the no wind results were used as a reference. The initial conditions for both cases are listed in Table 4. The initial values were taken from a hybrid simulation of a C-135 aircraft undergoing an automatic approach to landing on a 2.8 deg glideslope.[3] A conventional operational autopilot was modelled in that simulation which included glideslope and localizer capture, glideslope and localizer tracking, and flare. The values of the states at the beginning of flare were used as the initial conditions. The same wind conditions described in this investigation were used to obtain the initial values for the second case. The second case, then, reflects the effect of winds through the whole approach. This permits a realistic evaluation of the optimal control law in an automatic approach and landing. The first case, on the other hand, isolates the performance of the optimal flare law; a direct comparison of the response to various wind conditions can be made. Both cases are described by plots of the flare trajectories which are changes in altitude versus range, the nine states versus time, and the two control variables versus time.

TABLE 4

INITIAL CONDITIONS FOR FLARE

		CASE I	CASE II			
		All Wind Conditions	No Wind	Constant Wind	Linear Headwind Shear	Logarithmic Headwind Shear
q	(rad/sec)	-.0002735	-.0002735	.0002735	-.0001172	.0009766
θ	(rad)	-.04957	-.04957	-.04792	-.03906	-.03974
w_{as}	(ft/sec)	-.5117	-.5117	-.1367	1.762	2.715
u_{as}	(ft/sec)	.7	.7	.35	-3.38	-6.99
δT	(lbs)	-4738	-4738	-8558	-1590	-5496
r	(ft)	-2190	-2190	-2190	-2165	-2215
$\dot{h}$	(ft/sec)	-12.29	-12.29	-9.96	-11.48	-11.44
h	(ft)	69.99	69.99	69.71	69.94	69.48
δe	(rad)	.009886	.009886	.007977	.006749	.007704

4.2 First Case: Simulation with Identical Initial Conditions

The flare trajectories for the first case are shown in Figure 2. Flare starts at 70 ft. Since the altitude of the center of gravity is plotted, touchdown occurs at 10 ft. The optimal no wind profile is a smooth arresting of sink rate which would be acceptable to a pilot. The linear and logarithmic headwind profiles are very similar and do not vary too much from the no wind profile. The steady headwind profile is several feet below the no wind case. This is to be expected since a path is not tracked and a high wind continues for the whole flare. The steady wind trajectory is acceptable; in fact, this profile is similar to a manual landing in the same wind conditions. The touchdown points for all winds are close to one another. The slopes at the ends of the trajectories indicate that the sink rates are also similar. More specific information about the profiles and end conditions is provided by plots of the state variables.

Pitch rate of the aircraft is shown in Figure 3. The no wind curve stays positive; the aircraft is rotating up in the flare to arrest sink rate and decrease airspeed. The optimal computation yields an oscillation toward the end of the flare; however, pitch rate is positive and the maximum value is less than .02 rad/sec. The linear headwind curve is very similar to the no wind curve in oscillations and overall time for flare. This occurs since the linear headwind at flare initiation is not too great and it shears to zero; its value is 6.08 ft/sec. The logarithmic headwind at flare is much higher; its value is 25.07 ft/sec. This wind causes a a considerably slower groundspeed which results in a longer flare time in

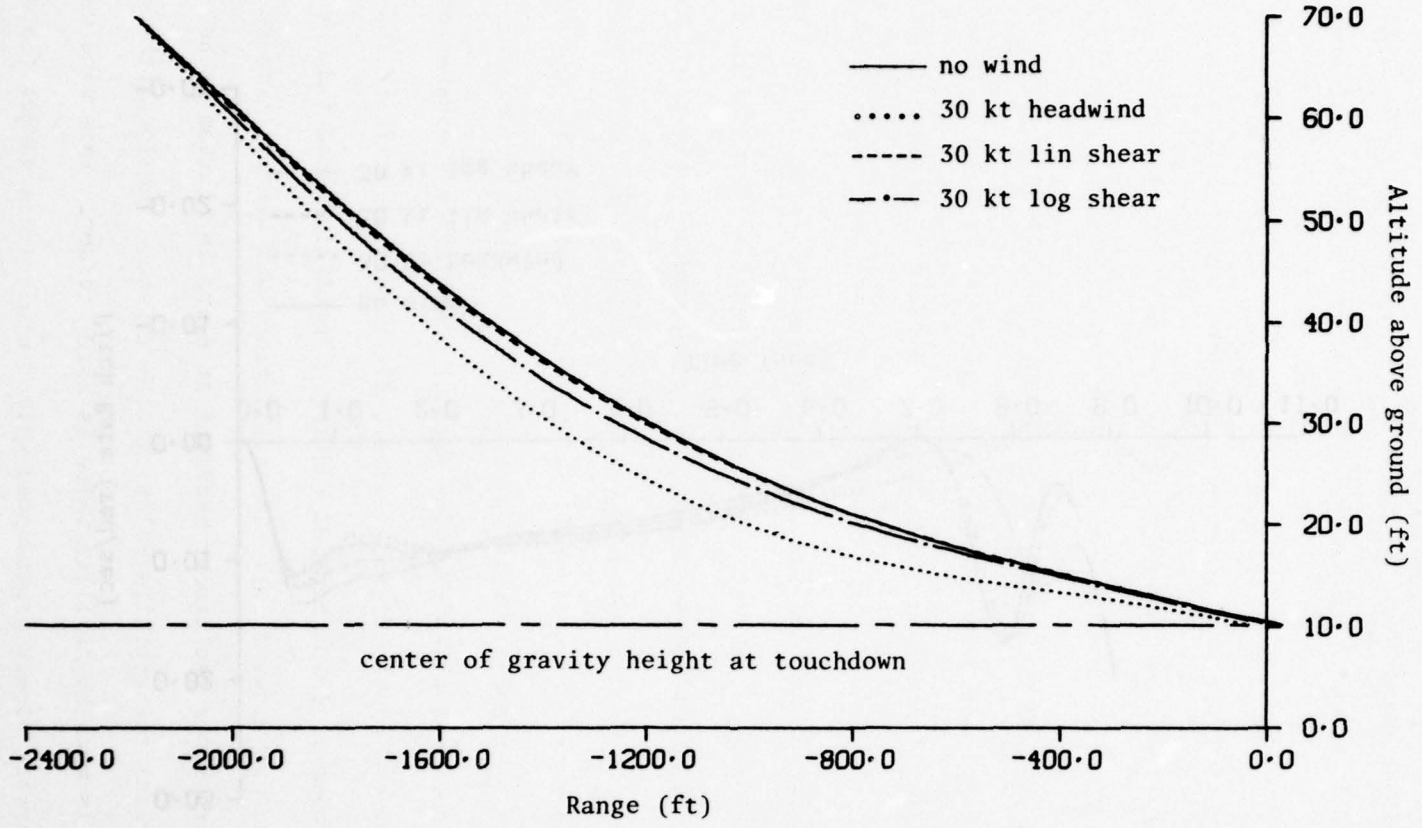

Figure 2. Range Trajectories with Identical Initial Conditions for Various Winds.

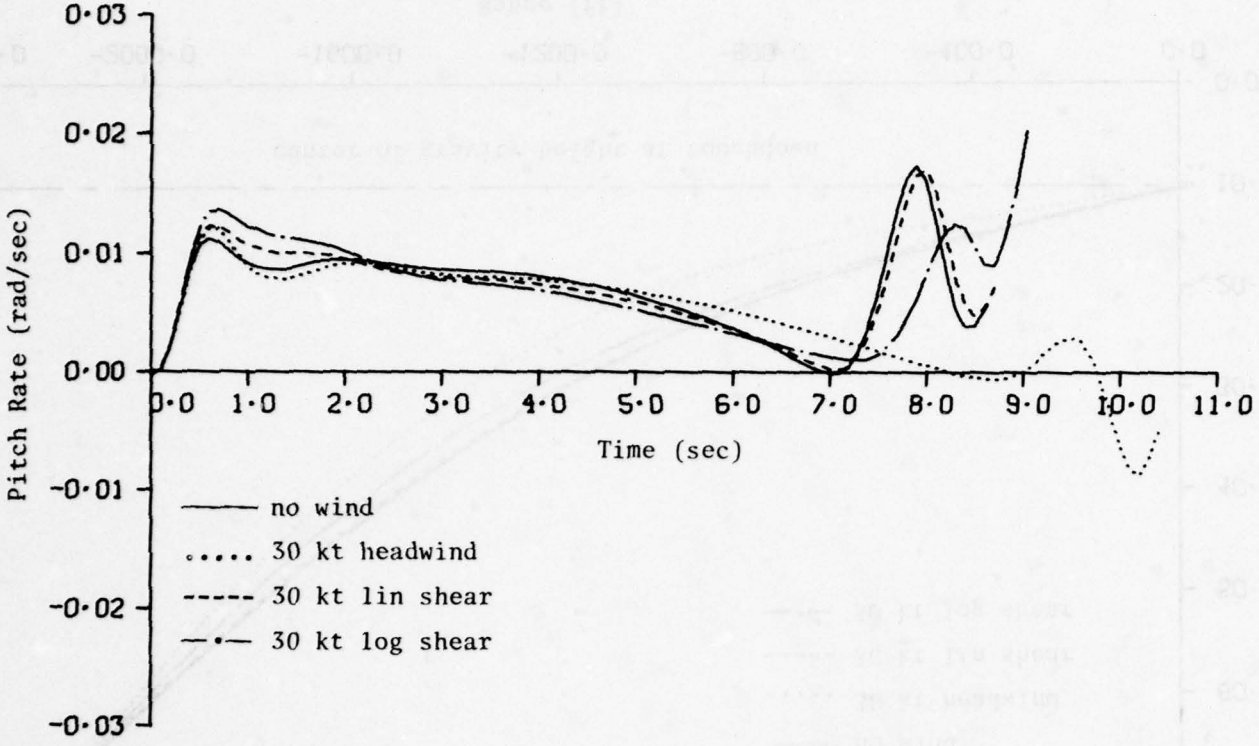

Figure 3. Pitch Rates with Identical Initial Conditions for Various Winds.

order to meet the range constraint. The logarithmic headwind also shears more quickly in the flare. Thus, the logarithmic headwind curve differs noticeably from the no wind case. The constant 50.67 ft/sec headwind causes an even slower groundspeed with a correspondingly longer flare time. Pitch rate toward the end of the flare is smaller than in the no wind case in order to keep the pitch angle of the aircraft smaller; this smaller pitch angle permits a stretching of the path in time so that the terminal conditions can be met. In the above discussion, it should be noted that airspeed is tracked, but altitude is not tracked.

Perturbation pitch angle is shown in Figure 4. As indicated by pitch rate, pitch angle increases during the flare. The constant headwind curve indicates the stretching of the flare for that wind condition; even though the perturbation pitch angle is very slightly negative, the positive nonperturbation value yields a positive pitch angle at touchdown for the aircraft. A positive value for pitch angle is needed to have initial ground contact with the main landing gear and not the nose wheel.

Normal airspeed of the aircraft is shown in Figure 5. The constant headwind case stands out again; the downward airspeed is considerably lower toward the end of flare than in the other conditions. As before, this permits the satisfaction of the terminal constraints.

Perturbation longitudinal airspeed is plotted in Figure 6. It should be noted that a perturbation longitudinal airspeed profile is tracked. The no wind curve closely follows the desired airspeed. The linear headwind curve is again very near to the no wind curve. The greater shear in the logarithmic headwind case is evident; during the first few seconds of

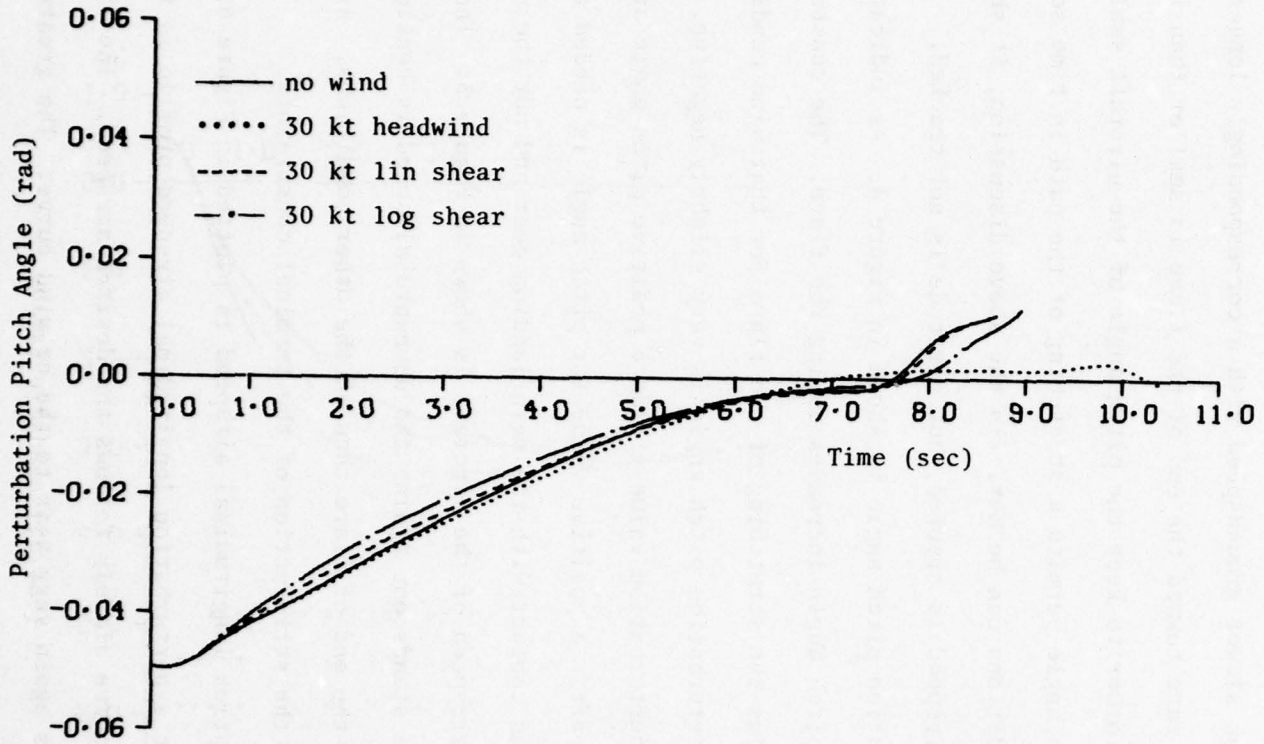

Figure 4. Perturbation Pitch Angles with Identical Initial Conditions for Various Winds.

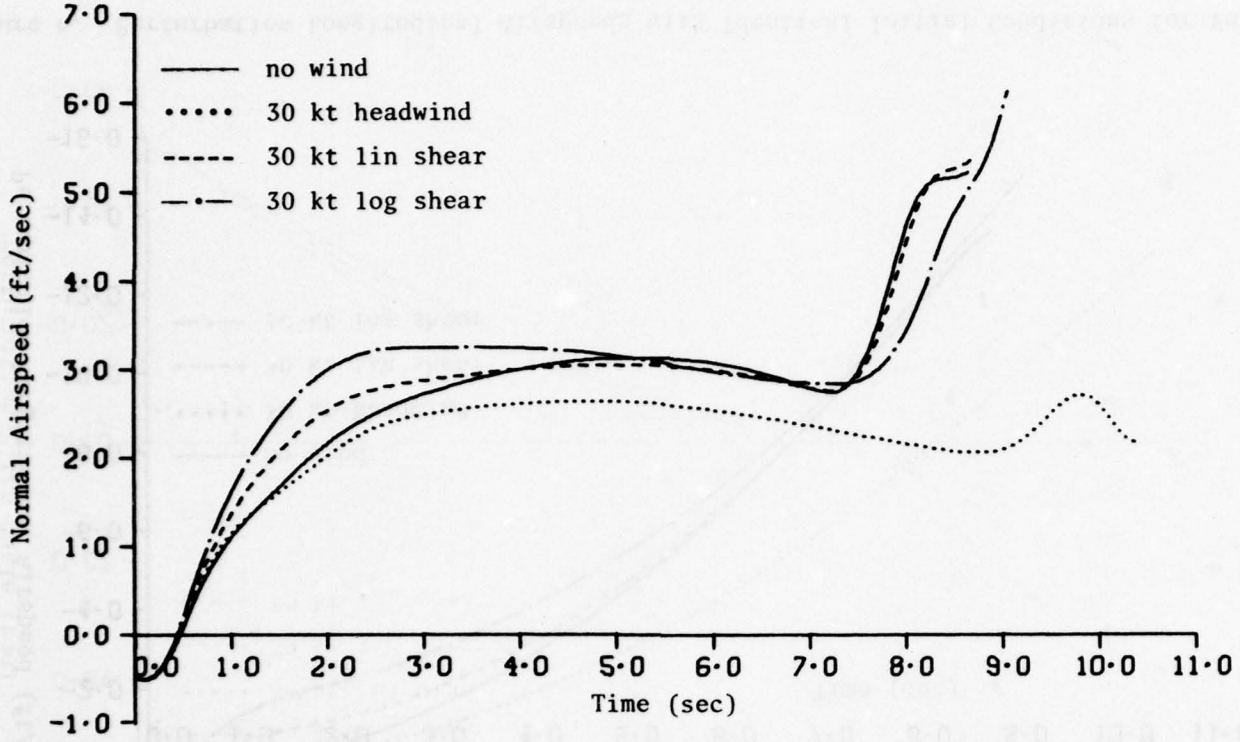

Figure 5. Normal Airspeeds with Identical Initial Conditions for Various Winds.

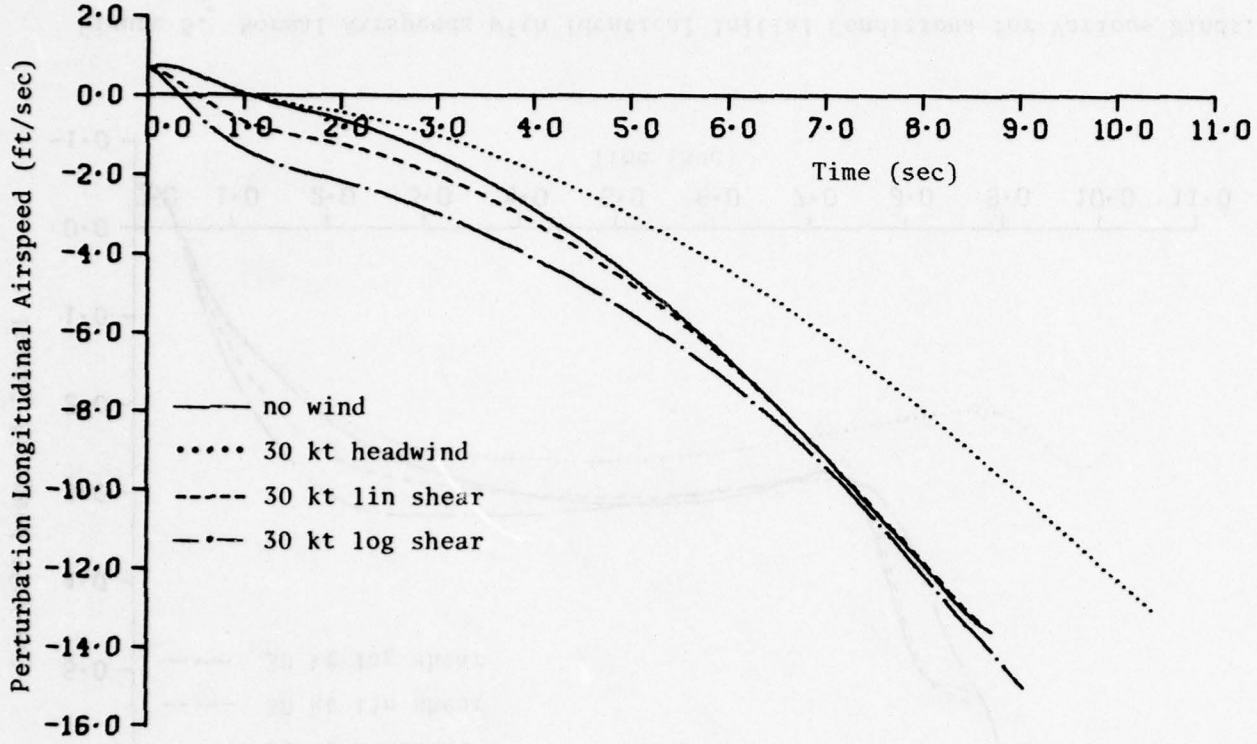

Figure 6. Perturbation Longitudinal Airspeeds with Identical Initial Conditions for Various Winds.

flare, the airspeed is about 2 ft/sec slower than desired. The airspeed approaches the desired profile in the latter part of the flare. However, lift is decreased sufficiently to result in a slightly lower logarithmic headwind trajectory as shown in Figure 2. The constant wind airspeed curve is not very different from the desired no wind curve when the lower groundspeed is considered; it should be noted that the optimal gains are applied based on range from a desired touchdown point. The terminal airspeeds for all wind conditions are near the desired value of -13.8 ft/sec.

Change in thrust is shown in Figure 7. The decrease in thrust for the no wind curve is necessary to attain the desired airspeed profile. The increase in thrust for the linear and logarithmic headwind curves is needed to overcome the airspeed loss due to wind shear; the greatest thrust increase is for the larger logarithmic headwind shear. The constant headwind curve reflects the lower groundspeed.

Range is plotted in Figure 8. The spread in the curves is due to differences in groundspeed. As the curves indicate, longitudinal dispersion is quite small. Specifically, the no wind, linear headwind shear, logarithmic headwind shear, and constant headwind terminal range values are 31.7, 30.1, 11.1, and -38.9 ft. The total longitudinal dispersion is 70.6 ft.

Sink rate is shown in Figure 9. The no wind, linear headwind shear, and logarithmic headwind shear curves are very similar; terminal values are -2.30, -2.31, and -2.42 ft/sec. The constant wind curve reflects the stretching of the flare due to the much slower groundspeed; the terminal value is -2.25 ft/sec. The total difference in sink rates at touchdown is .17 ft/sec.

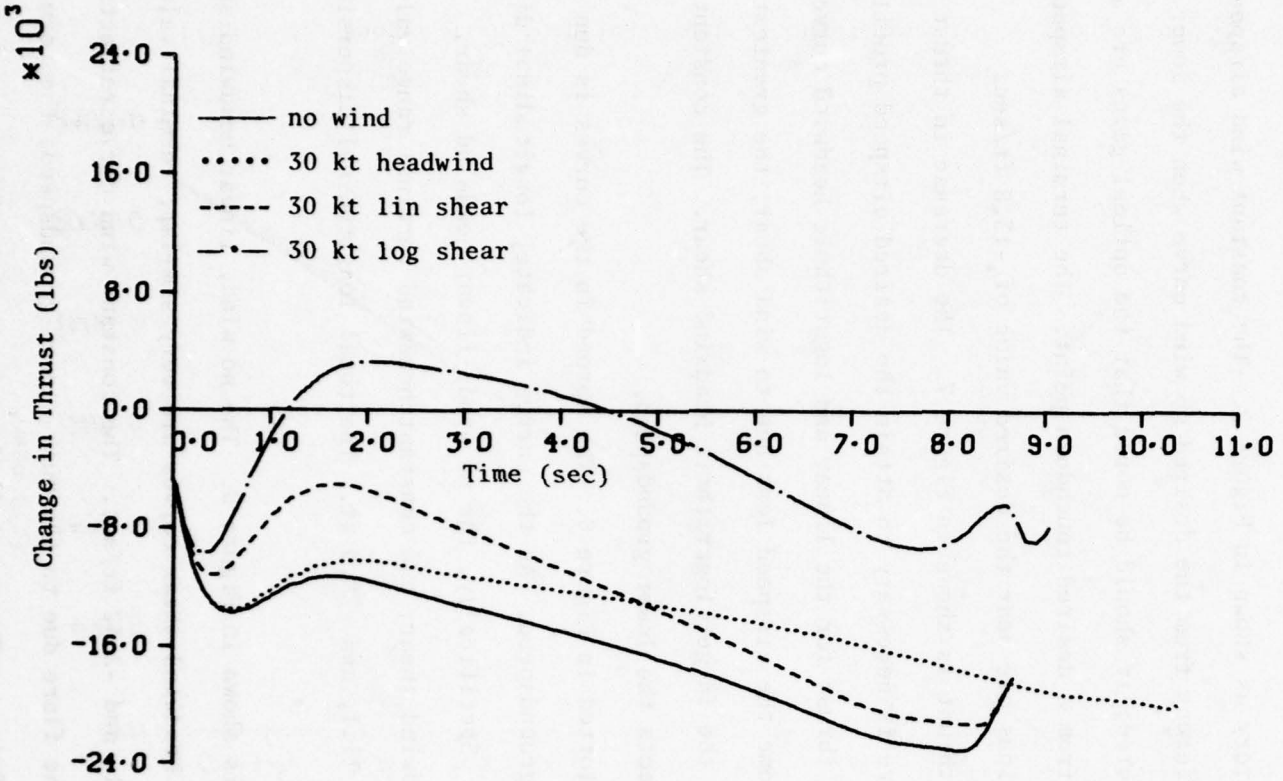

Figure 7. Changes in Thrust with Identical Conditions for Various Winds.

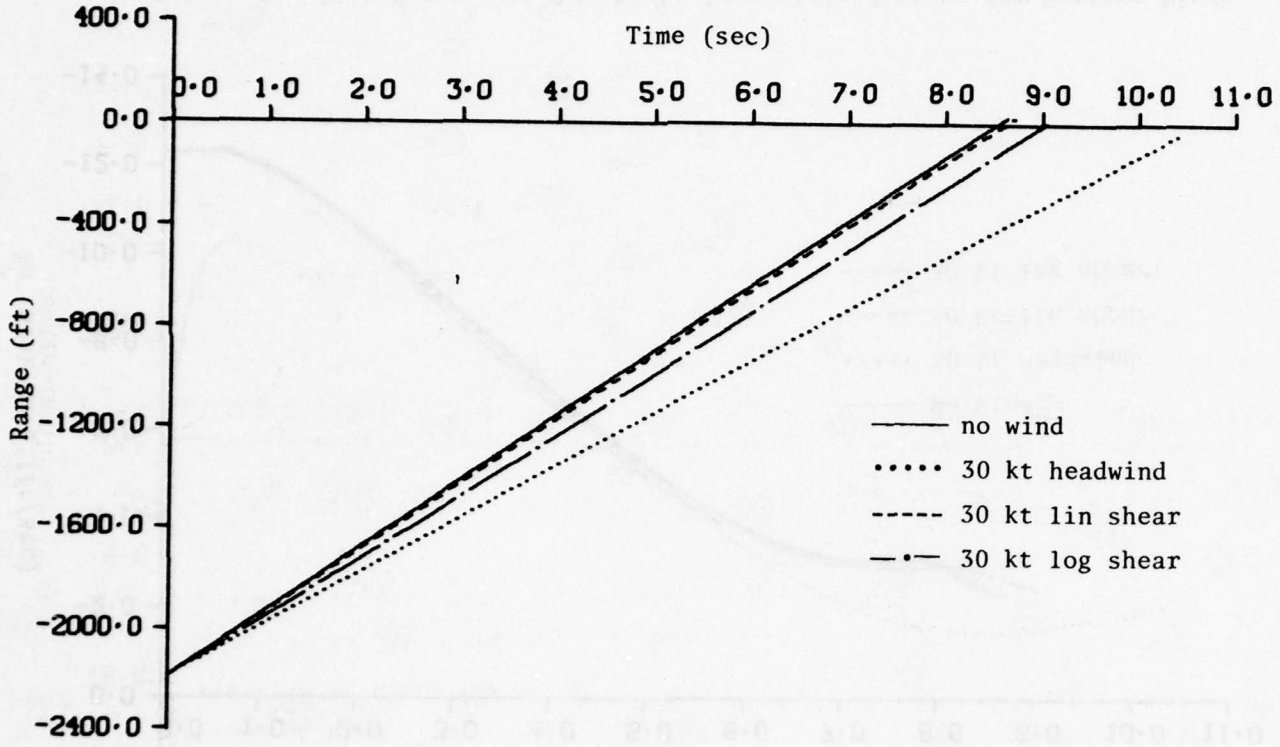

Figure 8. Ranges with Identical Initial Conditions for Various Winds.

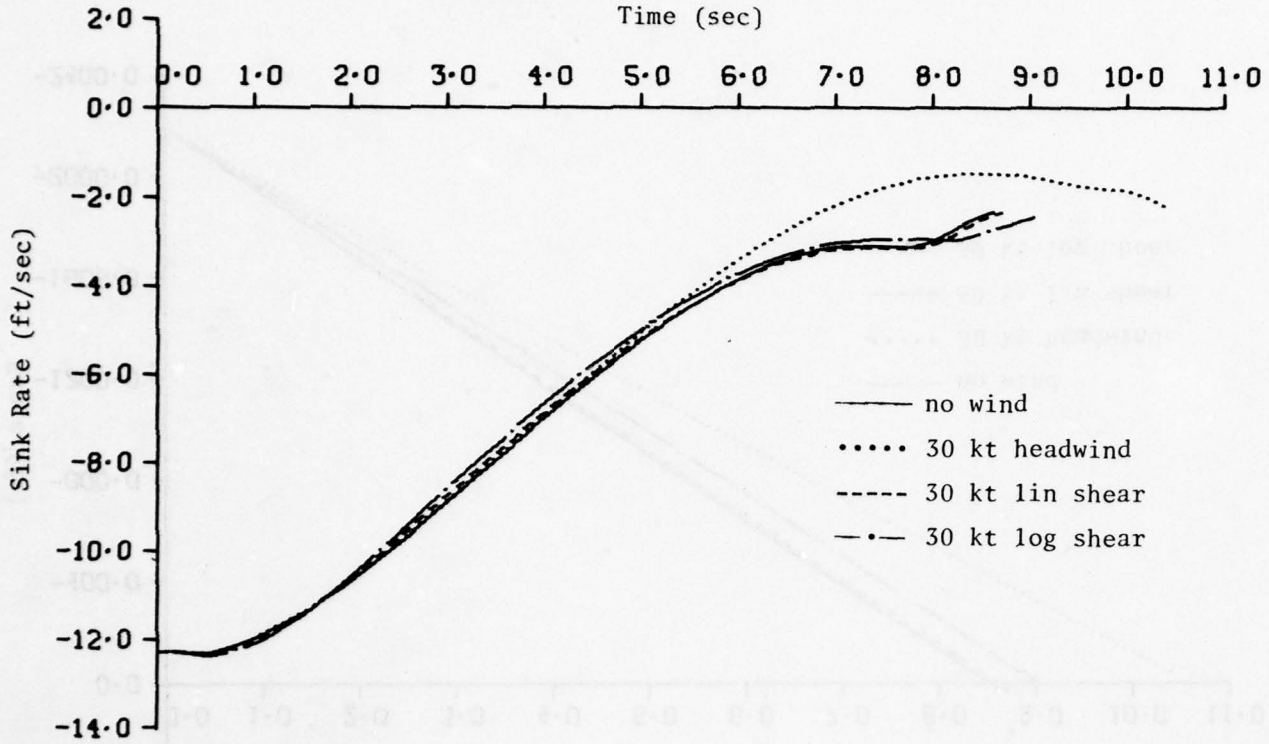

Figure 9. Sink Rates with Identical Initial Conditions for Various Winds.

The trajectory profiles with respect to time are shown in Figure 10. The curves are smooth and the effect of decreased groundspeed is evident. Touchdown occurs at 10 ft.

Change in elevator angle is plotted in Figure 11. The elevator angle increases in order to increase the pitch angle of the aircraft. The elevator angles for the various wind conditions are generally lower than the no wind curve; additional nose up rotation of the aircraft is caused by the increase in thrust. The constant wind curve has a lower maximum angle in order to stretch the flight path. In order to meet all constraints, the optimal control solution yields an oscillation in the elevator toward the end of flare. As the curves for pitch rate and perturbation pitch angle indicate, this oscillation does not result in objectionable rotation of the aircraft. It should be noted that the rate of elevator movement is feasible.

Aircraft controls are plotted in Figures 12 and 13. Change in elevator angle lags the control column angular displacement shown in Figure 12. Change in thrust lags the throttle angular displacement shown in Figure 13. It should be noted that the jittery behavior of the controls which is evident in some of the curves does not show up in the elevator angle or thrust. In actual implementation, it also would not show up in the cockpit since the control column and throttles move according to the output of servos.

4.3 Second Case: Simulation with Different Initial Conditions

This case is a more difficult test since the wind shears are in effect from 1000 ft and cause a substantial deficit in airspeed at flare

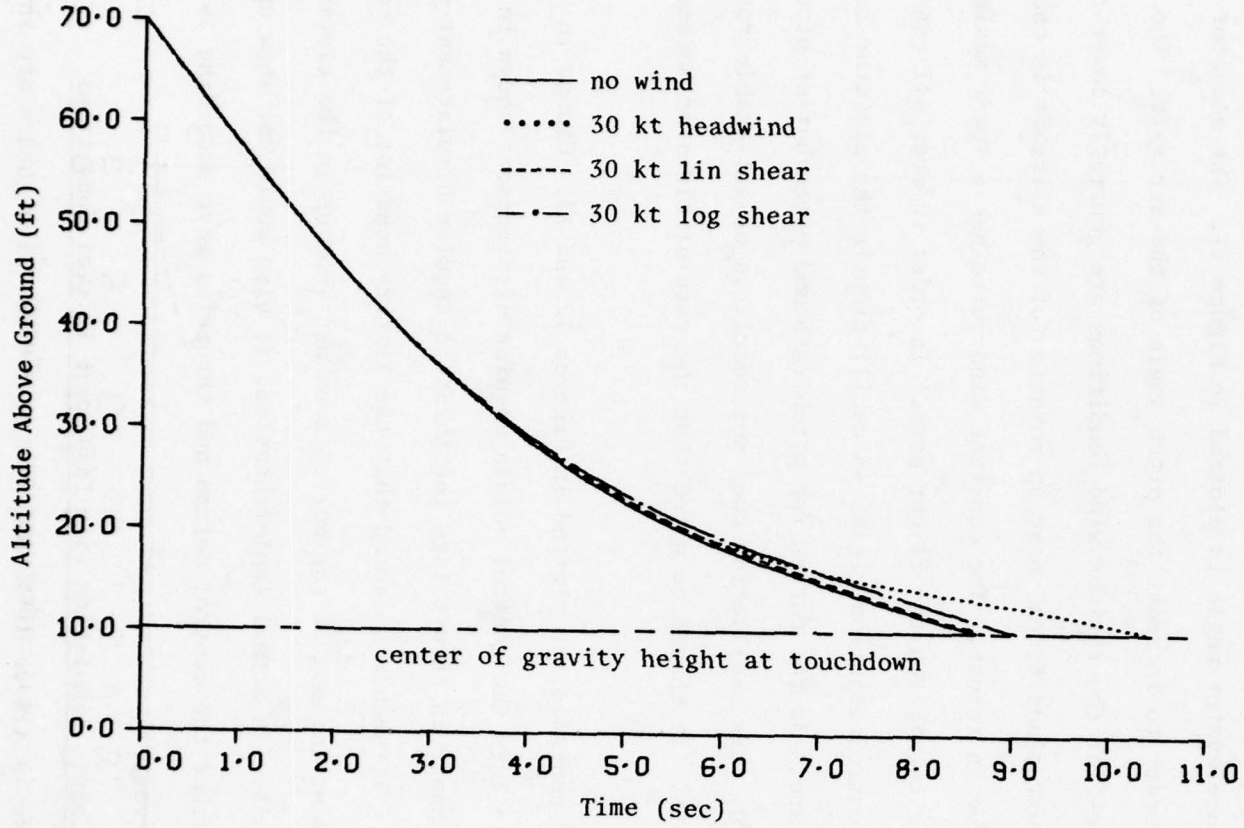

Figure 10. Time Trajectories with Identical Initial Conditions for Various Winds.

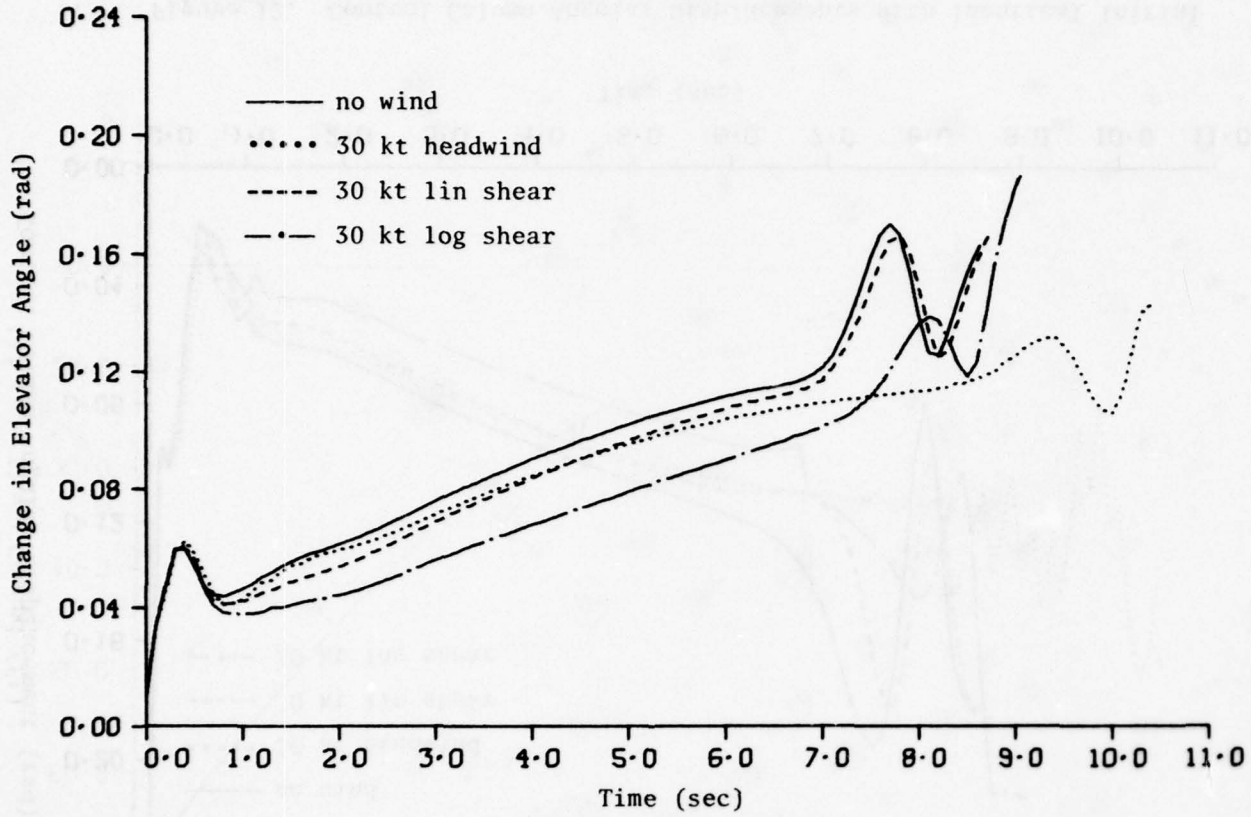

Figure 11. Changes in Elevator Angle with Identical Initial Conditions for Various Winds.

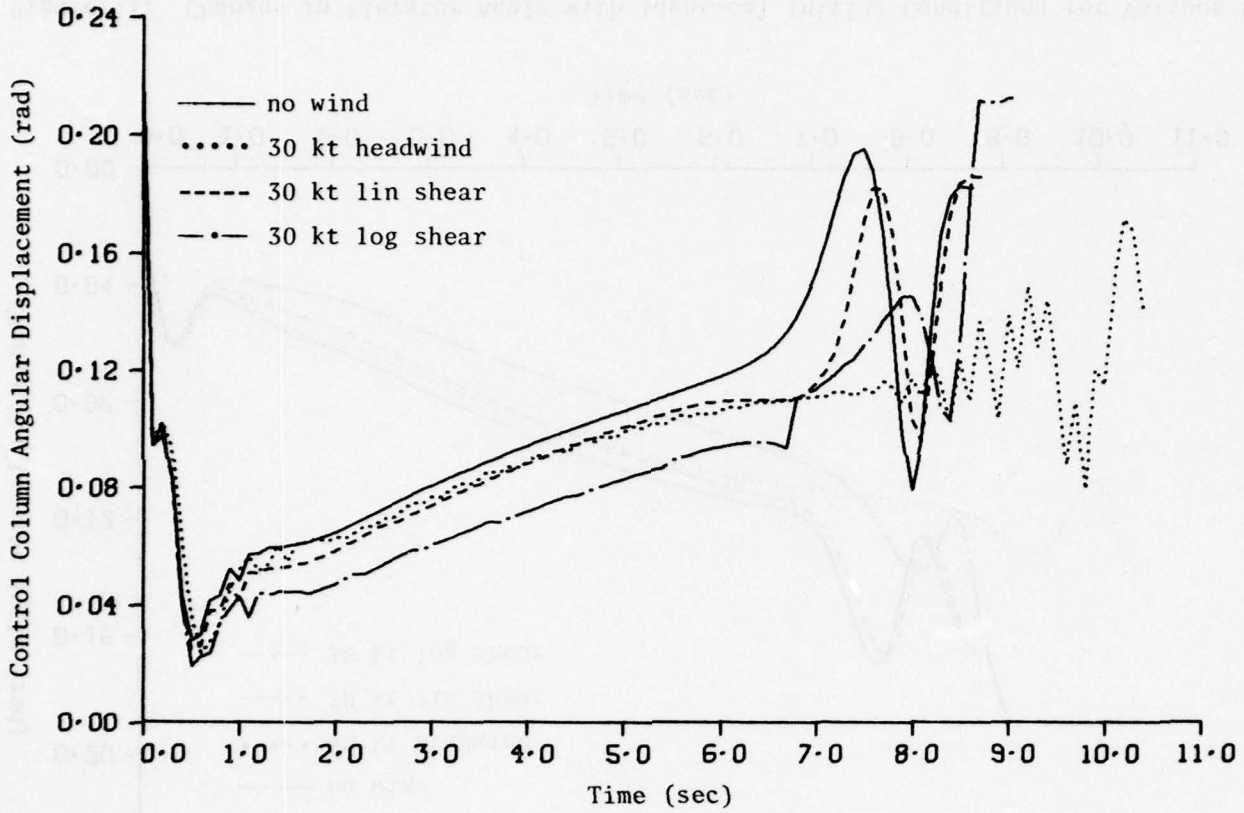

Figure 12. Control Column Angular Displacements with Identical Initial Conditions for Various Winds.

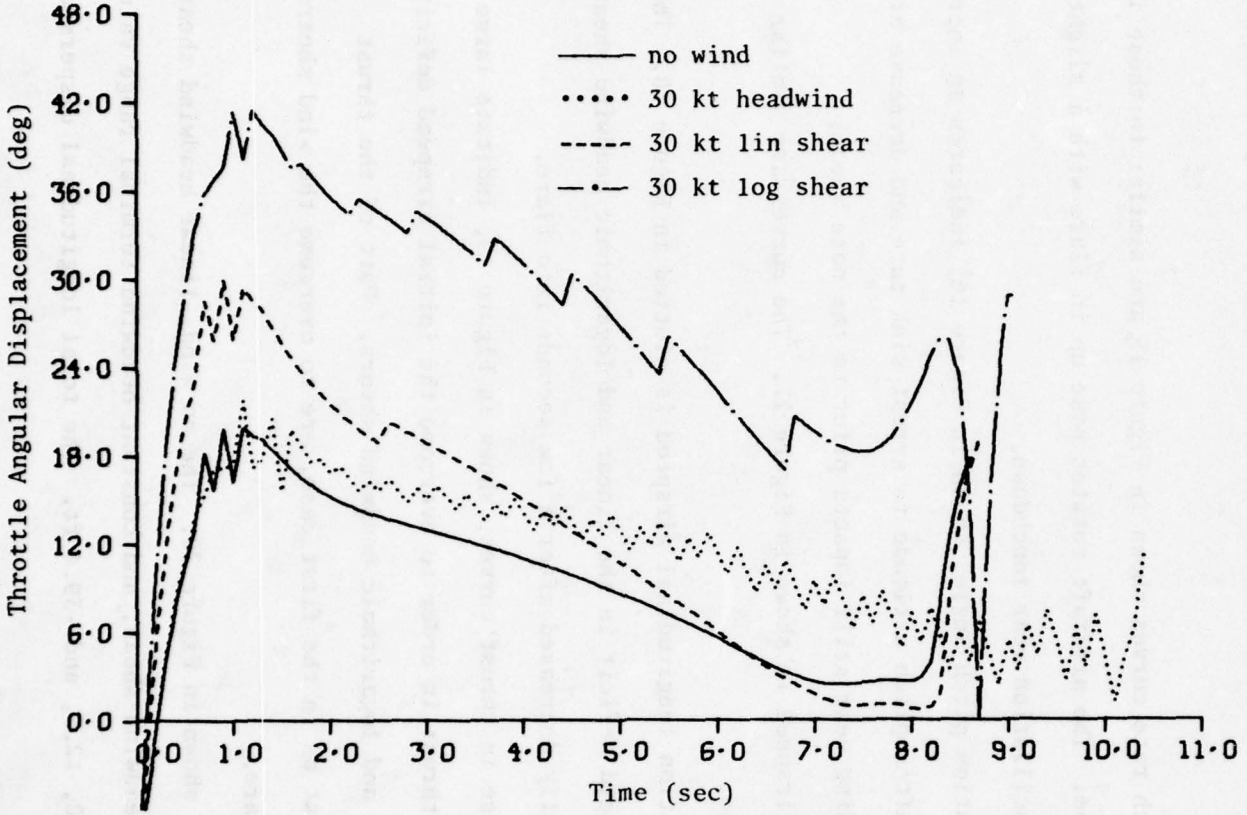

Figure 13. Throttle Angular Displacements with Identical Initial Conditions for Various Winds.

initiation. The flare trajectories for the second case are shown in Figure 14. Even with the airspeed deficit, the optimal control law still yields an acceptable smooth profile that meets the terminal constraints.

The pitch rate curves shown in Figure 15 are similar to those in the first case. The aircraft rotates nose up in flare with a slight pitch rate oscillation near touchdown.

Perturbation pitch angle, shown in Figure 16, indicates an increase in the aircraft's pitch attitude to arrest sink rate and decrease airspeed. The main landing gear still impacts prior to the nose wheel.

Normal airspeed is shown in Figure 17. The curves are similar to the first case.

Perturbation longitudinal airspeed is plotted in Figure 18. The initial airspeed deficit in the linear and logarithmic headwind shears is substantially decreased after a few seconds into flare.

The change in thrust curves, shown in Figure 19, indicate large increases in thrust in order to overcome the initial airspeed deficit in the linear and logarithmic headwind shears. Part of the thrust increases, just as in the first case, are to overcome the wind shears during the flare.

Range is shown in Figure 20. The no wind, linear headwind shear, logarithmic headwind shear, and constant headwind terminal range values are 31.7, 30.0, 12.5, and -39.4 ft. The total longitudinal dispersion is 71.1 ft.

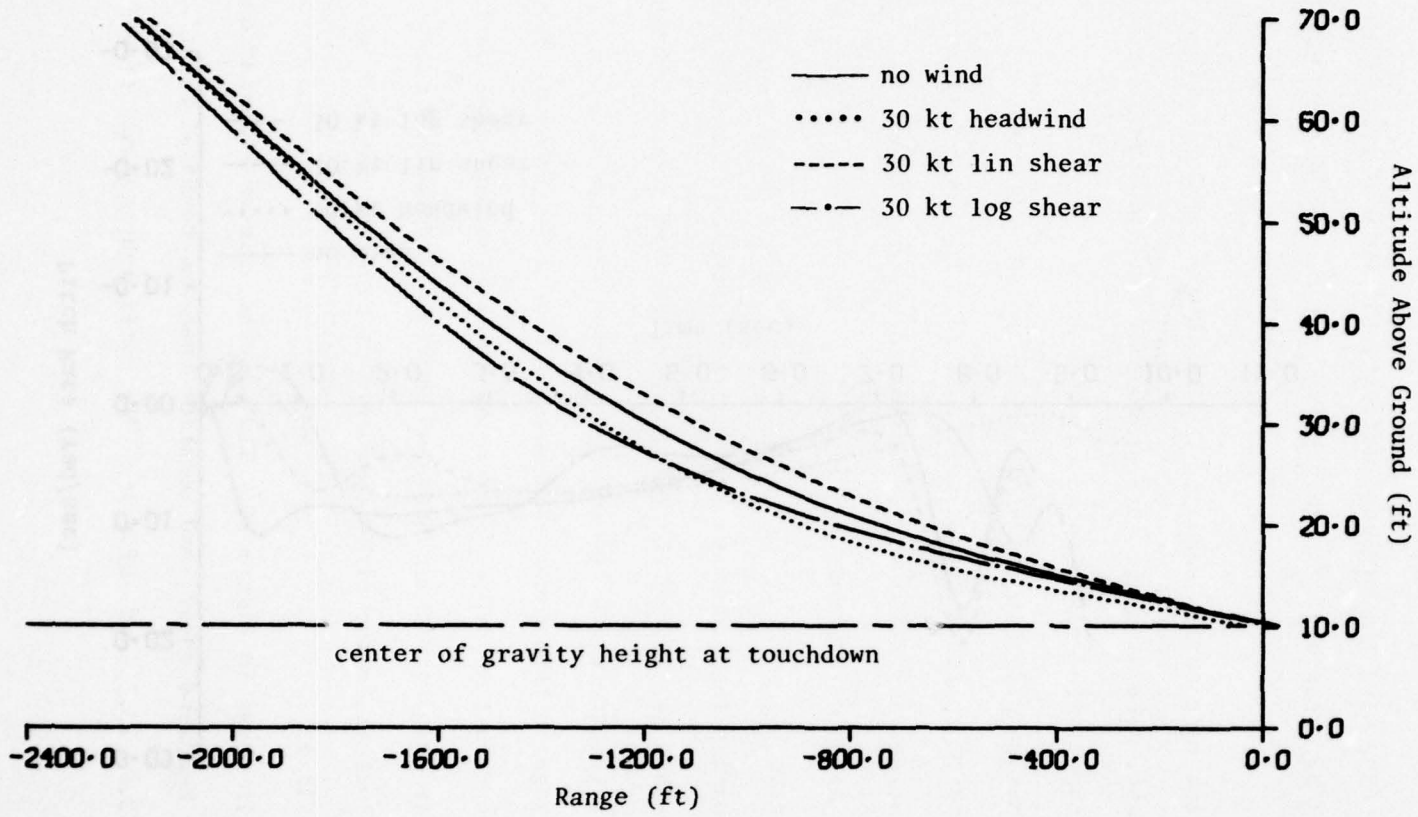

Figure 14. Range Trajectories with Different Initial Conditions for Various Winds.

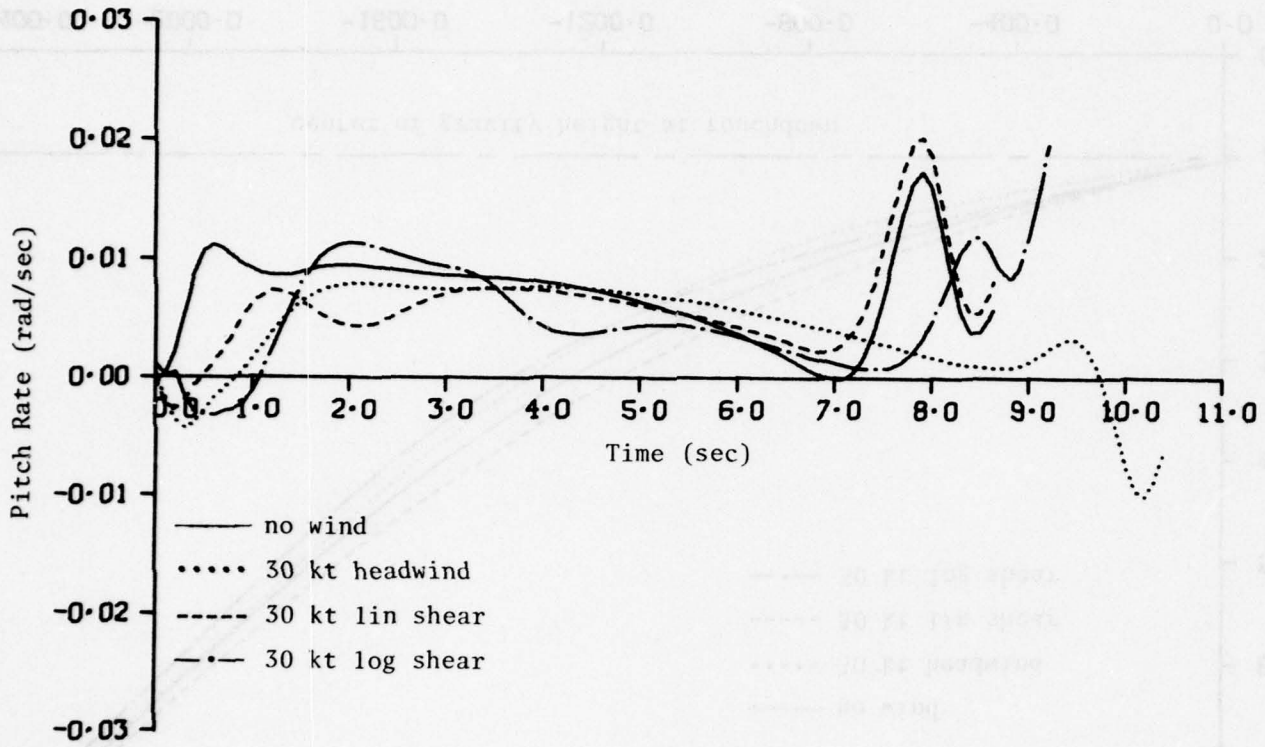

Figure 15. Pitch Rates with Different Initial Conditions for Various Winds.

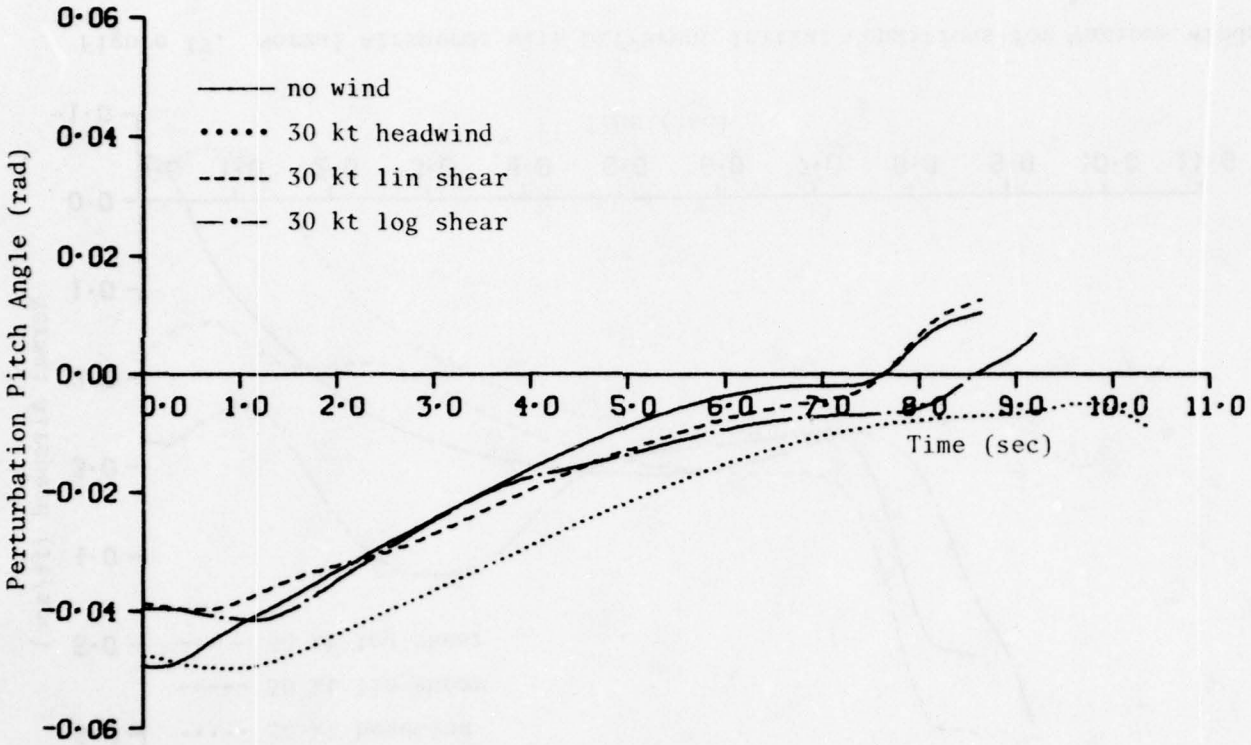

Figure 16. Perturbation Pitch Angles with Different Initial Conditions for Various Winds.

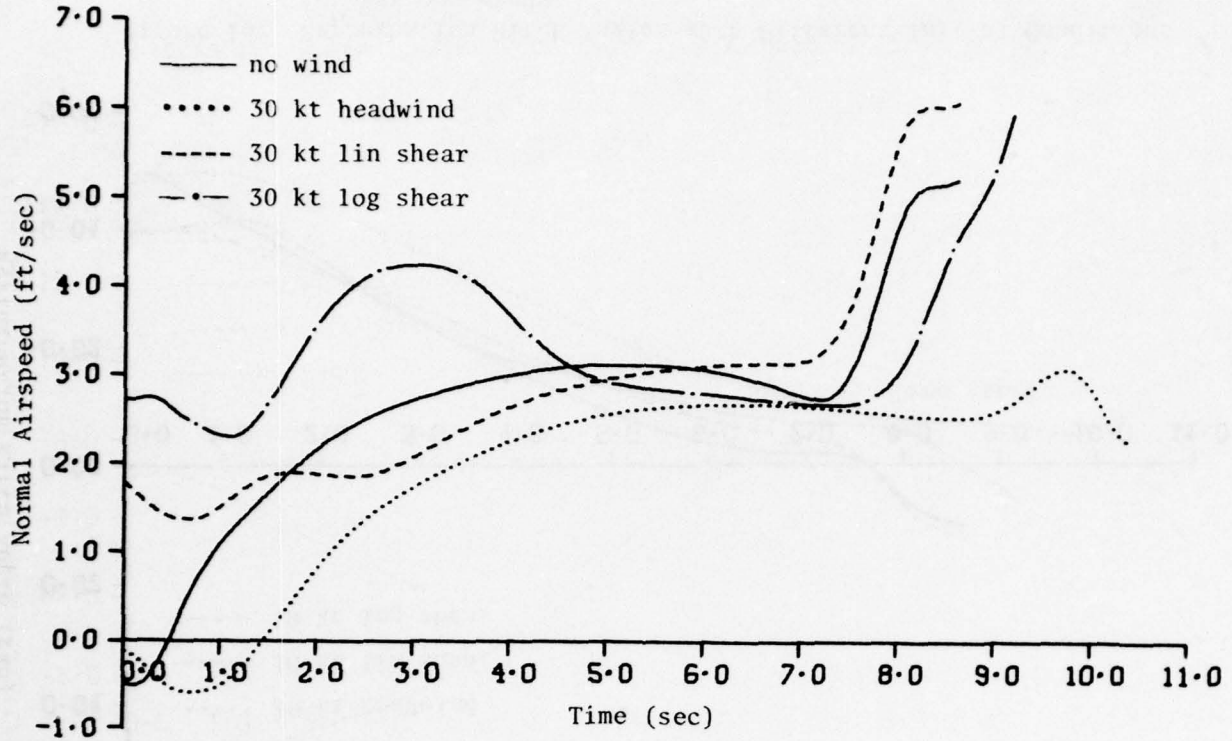

Figure 17. Normal Airspeeds with Different Initial Conditions for Various Winds.

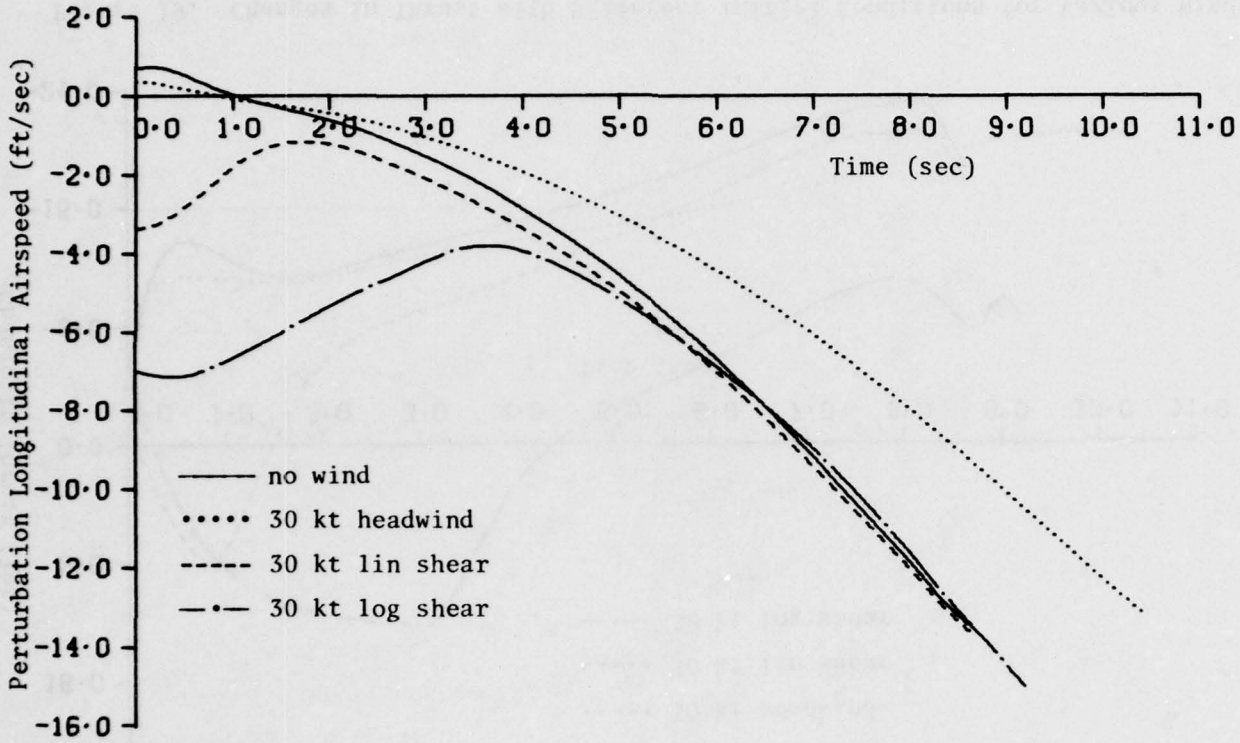

Figure 18. Perturbation Longitudinal Airspeeds with Different Initial Conditions for Various Winds.

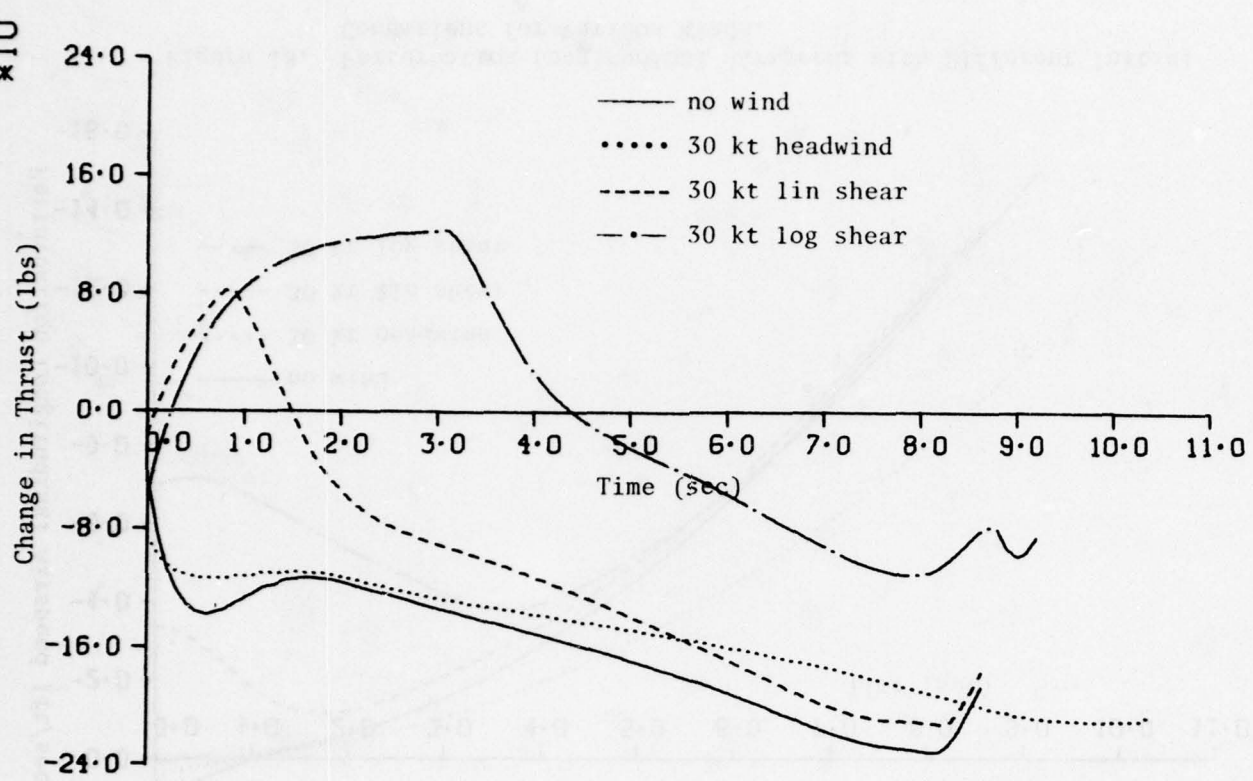

Figure 19. Changes in Thrust with Different Initial Conditions for Various Winds.

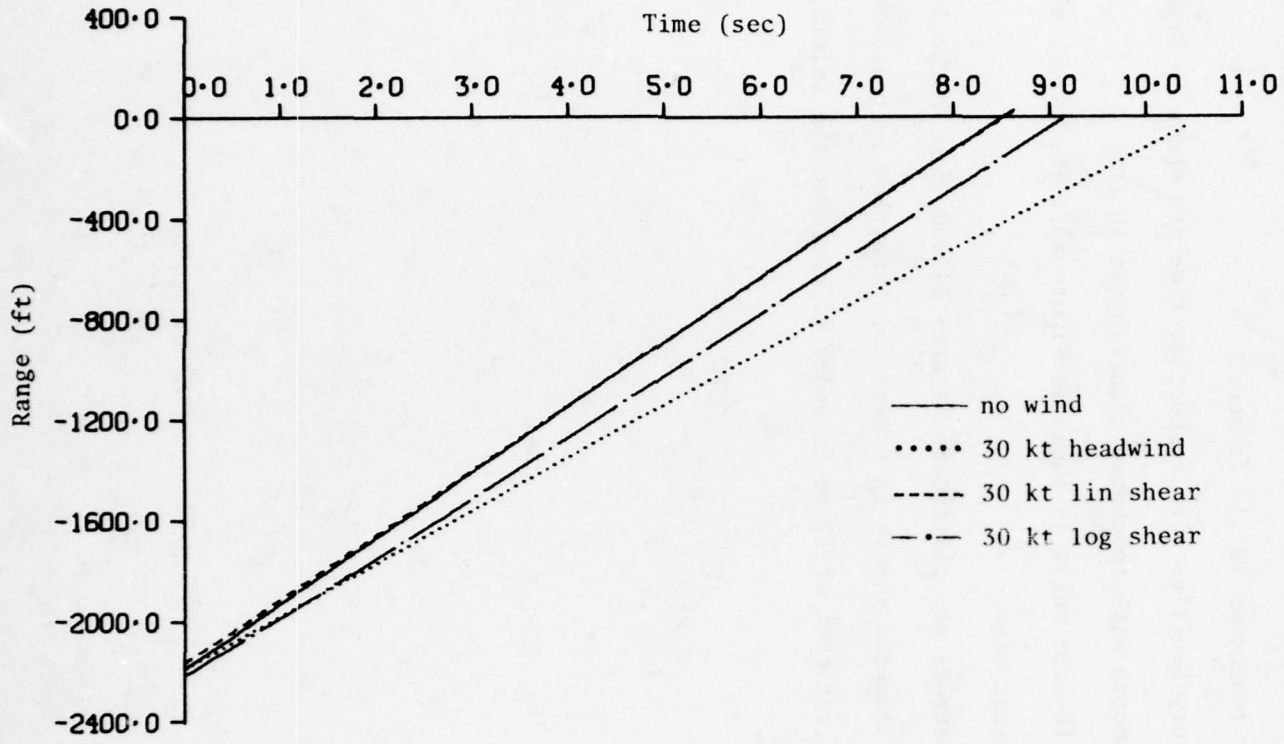

Figure 20. Ranges with Different Initial Conditions for Various Winds.

Sink rate is plotted in Figure 21. The no wind, linear headwind shear, logarithmic headwind shear, and constant headwind terminal sink rates are -2.30, -2.26, -2.42, and -2.25 ft/sec. The total difference in sink rates at touchdown is .17 ft/sec.

The trajectory profiles with respect to time are shown in Figure 22. The curves are smooth with touchdown occurring at 10 ft.

Change in elevator angle is shown in Figure 23. The curves are similar to the first case.

Aircraft controls are plotted in Figures 24 and 25. In the linear and logarithmic headwind shears in Figure 25, throttles increase to maximum in the first part of flare in order to overcome the initial airspeed deficit.

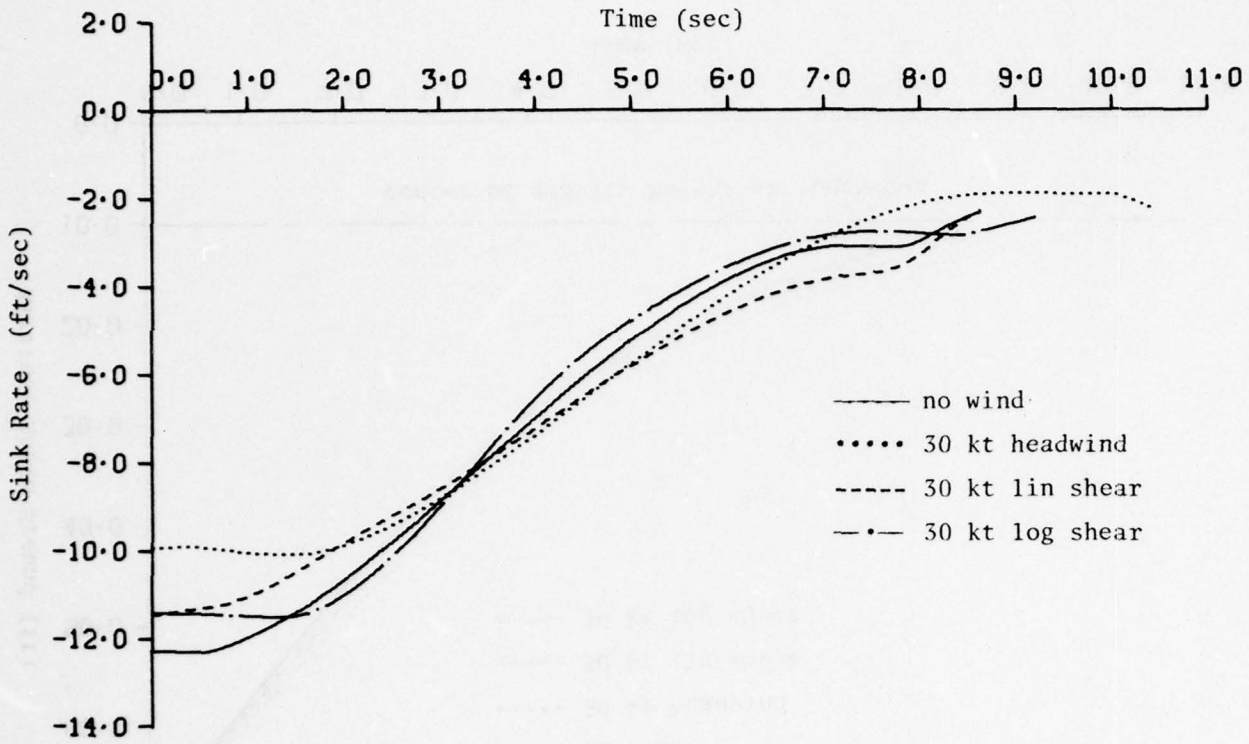

Figure 21. Sink Rates with Different Initial Conditions for Various Winds.

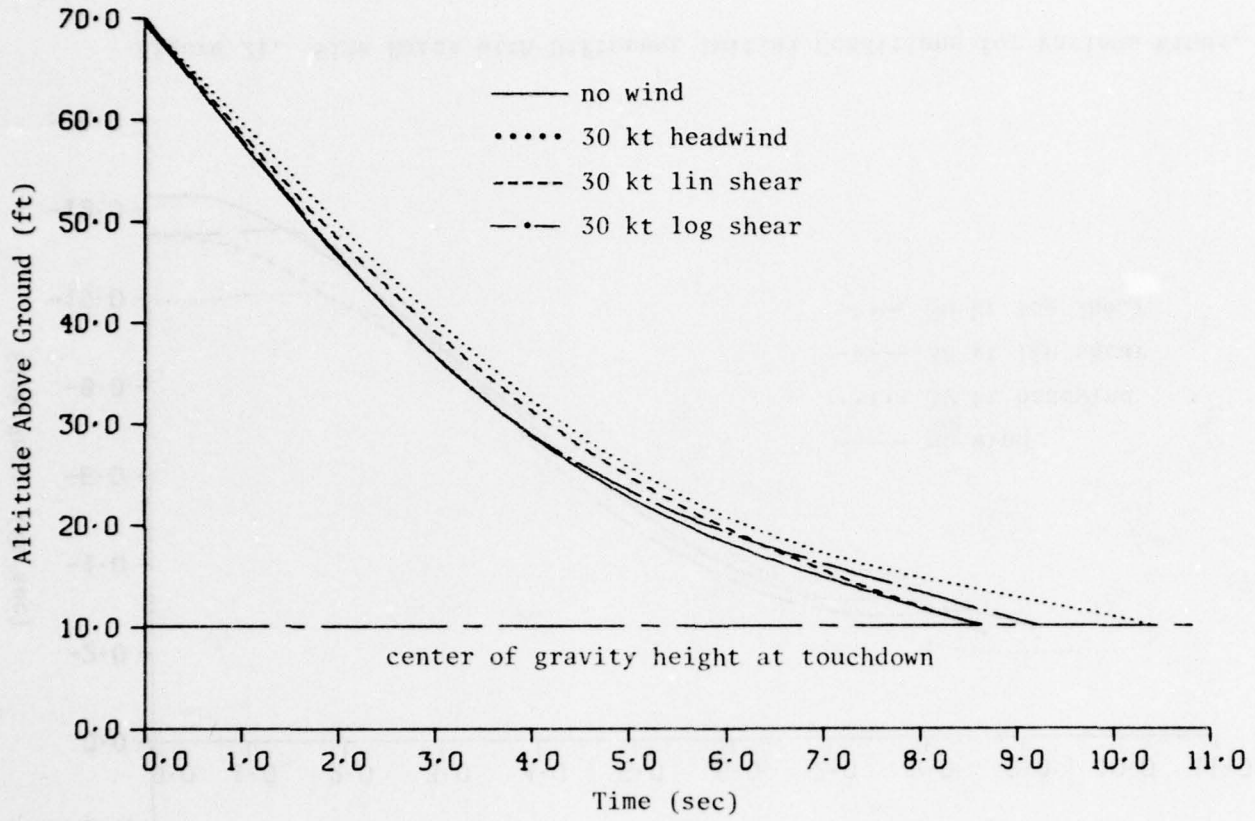

Figure 22. Time Trajectories with Different Initial Conditions for Various Winds.

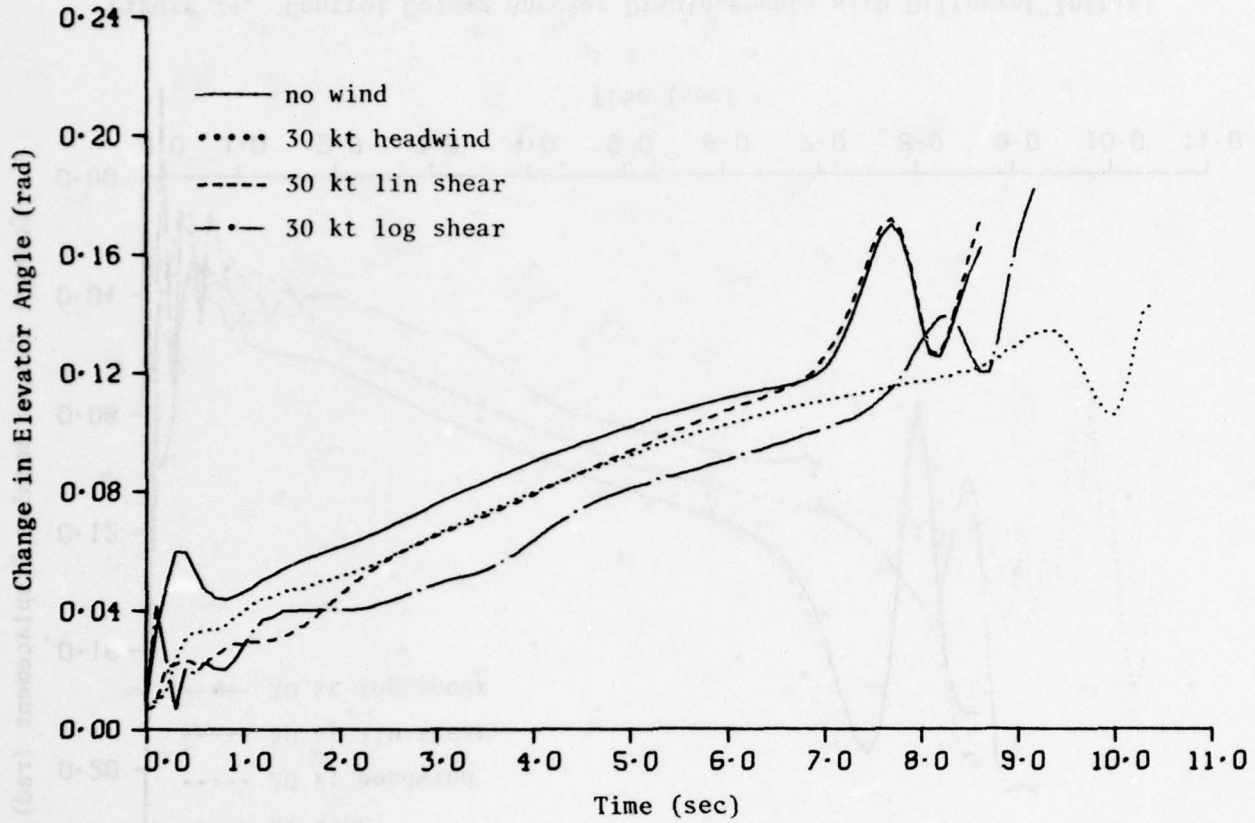

Figure 23. Changes in Elevator Angle with Different Initial Conditions for Various Winds.

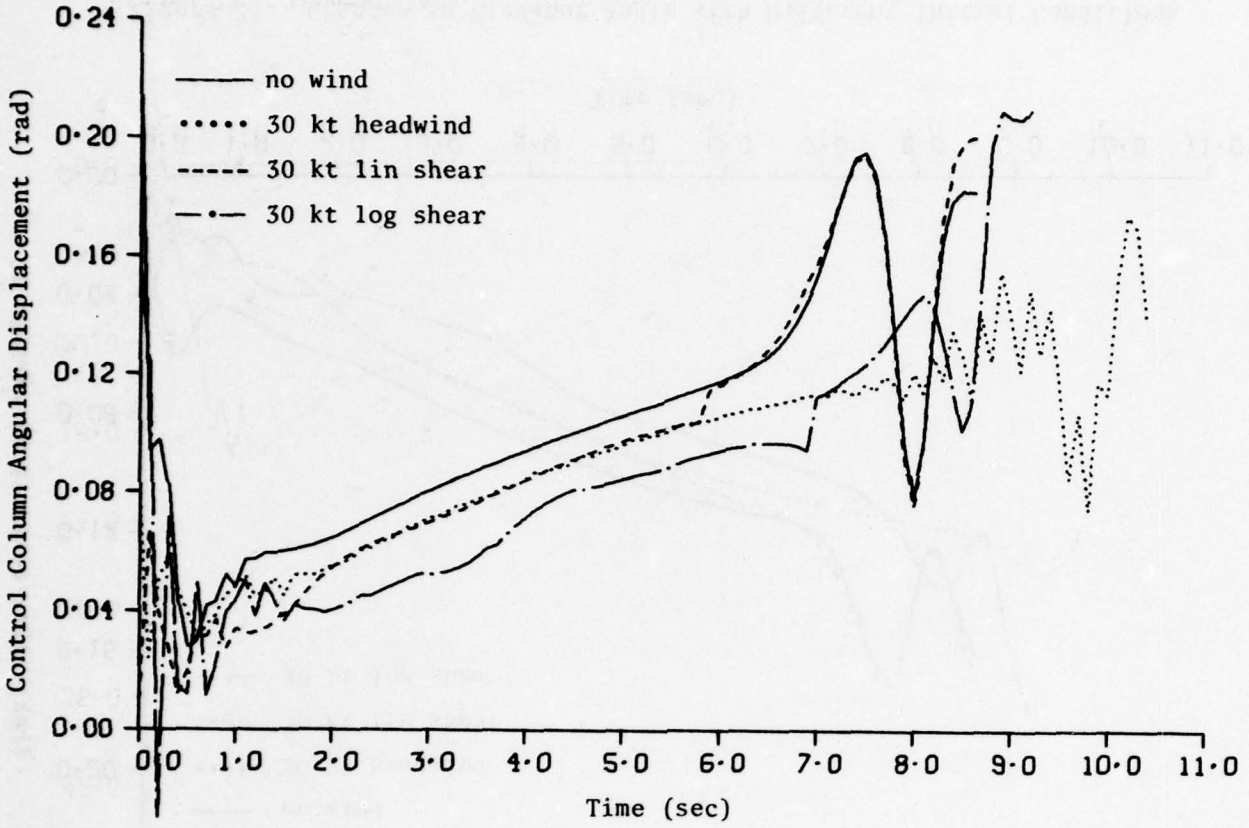

Figure 24. Control Column Angular Displacements with Different Initial Conditions for Various Winds.

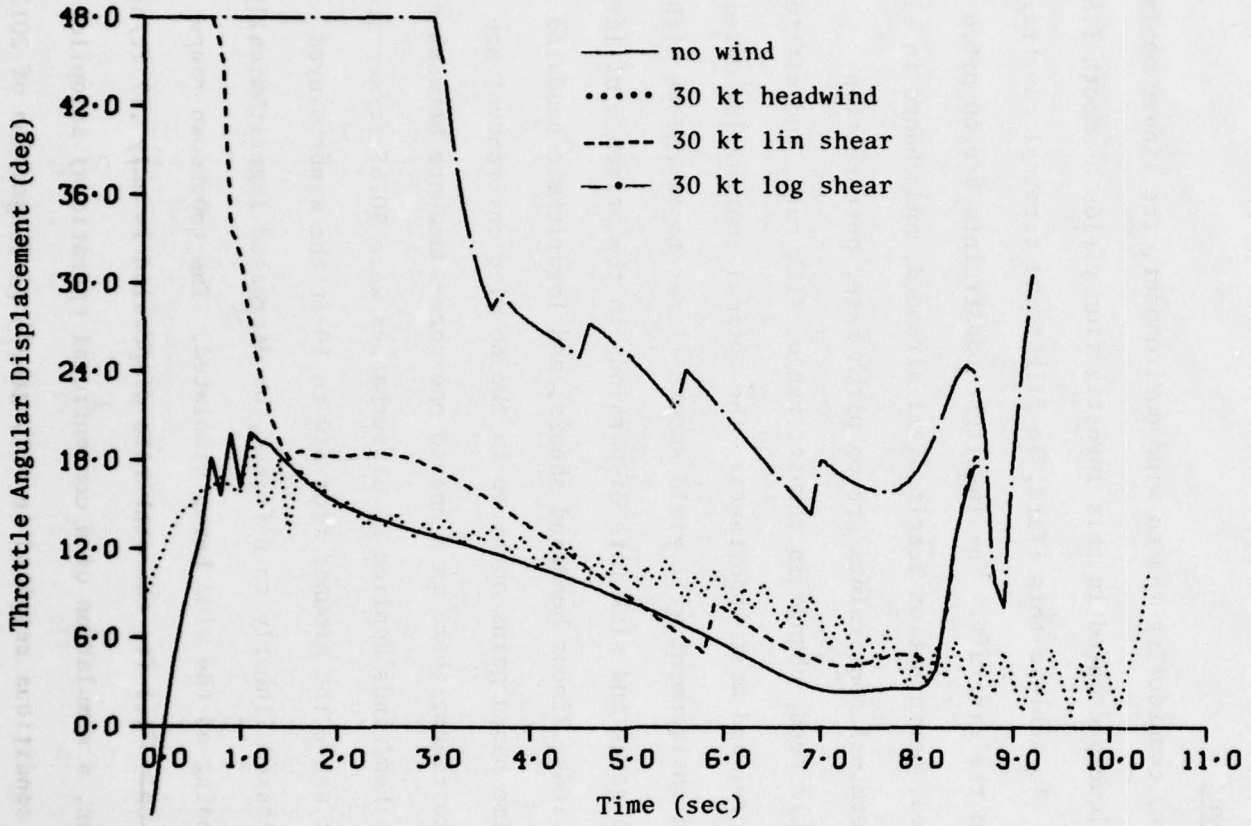

Figure 25. Throttle Angular Displacements with Different Initial Conditions for Various Winds.

SECTION 5

CONCLUSIONS AND RECOMMENDATIONS

5.1 Conclusions

Initially, considering the no wind environment, the linear optimal control technique presented in this investigation yields a smooth flare to touchdown. To achieve this flare, in-flight and terminal constraints were placed on the aircraft. The in-flight constraints are on pitch rate, normal airspeed, perturbation longitudinal airspeed, and change in elevator angle. The terminal constraints are on pitch rate, perturbation longitudinal airspeed, change in thrust, range, sink rate, and altitude.

Furthermore, and most importantly, the optimal control law developed in the no wind environment will yield smooth flares to touchdown with very small terminal range and sink rate dispersions in the presence of large constant headwinds, linear headwind shears, and logarithmic headwind shears. The optimal time based gains obtained in the no wind environment are applied with respect to range; there is a one to one correspondence between range and time. The headwinds applied as disturbances were 50.67 ft/sec from 1000 to 510 ft above the ground; from 510 to 10 ft the winds stayed constant, decreased linearly to 0 ft/sec, or decreased logarithmically to 0 ft/sec depending on the wind being simulated. The touchdown range dispersion is only 71.1 ft; the sink rate dispersion is only .17 ft/sec. As a comparison, a simulation of a conventional operational autopilot in the same wind conditions resulted in a longitudinal dispersion of 2017 ft and sink rate dispersion of 5.55 ft/sec with a maximum sink rate of -6.2 ft/sec.

The optimal linear control gains can be readily implemented in actual flight operations since only a few multiplication calculations are required to obtain the control signal and the gains are good for any initial conditions. It should be noted that nonlinear optimal control cannot be implemented due to the long computation time required to obtain a solution and the need to recompute gains for each set of initial conditions.

5.2 Recommendations

Since airspeed change during flare is substantial, the effect of changes in stability derivatives should be investigated. Also, a nonlinear simulation of the aircraft with linear optimal control gains should be accomplished prior to flight testing in order to verify all of the linearizing assumptions. This simulation should include a method to handle stabilizer trim. Also, tailwinds should be introduced to check the aircraft's response in these winds; the throttles should come off in tailwind shears since airspeed increases.

The response of the aircraft to gusts should be studied. It should be noted that a function of normal acceleration is weighted in-flight.

Optimal gains for various aircraft configurations, weights, and airspeeds will have to be obtained prior to flight test. In this study, only one aircraft condition was used. Provisions for efficiently storing the various sets of gains in a digital flight computer should be investigated.

As this study indicates, change of thrust is extremely important for small range and sink rate dispersions when in the presence of wind shears. In order to get a satisfactory comparison to classical flare techniques, the classical method should employ a very good automatic throttle system.

In order to have a smaller airspeed deficit at flare initiation when winds are present, improvements in glideslope tracking should be investigated. Also, localizer tracking and alignment should be investigated from the standpoint of effects to the optimal flare. Specifically, the nonlinear simulation that was mentioned previously should also include the lateral equations with crosswind disturbances.

It should be noted that the problem that was solved in this study is not just an improvement in aircraft flare performance. The optimal control technique presented here is good for placing an air vehicle at any point in space, with any terminal conditions, with any in-flight constraints, in any deterministic wind conditions; this can be done regardless of the vehicle's initial conditions.

REFERENCES

1. "Wind Factor Studied in Iberia Crash," Aviation Week and Space Technology, April 14, 1975, pp. 53-56.

2. "NTSB Studies Wind Shear as Factor in Eastern Crash," Aviation Week and Space Technology, June 30, 1975, p. 26.

3. Denaro, R. P., "The Effects of Wind Shear on Automatic Landing," AFFDL-TR-77-14.

4. Merriam, C. W., Optimization Theory and the Design of Feedback Control Systems, McGraw-Hill Book Company, Inc., New York, 1964.

5. Neal, G. L., "Flare Optimal Control: A Practical Time Domain Multivariable Problem," Report Number 523-0760774-00181M, Collins Radio Company, Cedar Rapids, Iowa, May 16, 1968.

6. Huber, R. R., Jr., "Optimal Control Aircraft Landing Analysis," AFFDL-TR-73-141, December 1973.

7. Trankle, T. L. and Bryson, A. E., Jr., "Autopilot Logic for the Flare Maneuver of STOL Aircraft," SUDAAD 494, Department of Aeronautics and Astronautics, Stanford University, Stanford, California, May 1975.

8. Blakelock, J. H., Automatic Control of Aircraft and Missiles, John Wiley and Sons, Inc., New York, 1965.

9. Bendix Navigation and Control Division R and D Report Number 7211-326, The Bendix Corporation, Teterboro, New Jersey, July 15, 1969.

10. Kirk, D. E., Optimal Control Theory, Prentice-Hall, Inc., Englewood Cliffs, New Jersey, 1970.

☆ U. S. GOVERNMENT PRINTING OFFICE: 1977 — 757-001/490